Spring 5-3-2024

Mesopelagic Microplastic Transport Interactions With the Biological Carbon Pump

Mikayla Clark
University of Maine, mikayla.clark1@maine.edu

MESOPELAGIC MICROPLASTIC TRANSPORT INTERACTIONS WITH THE BIOLOGICAL CARBON PUMP

By

Mikayla Clark

B.S. University of Alaska Southeast, 2020

M.S. University of Maine, 2024

A Thesis

Submitted in Partial Fulfillment of the

Requirements for the Degree of

Master of Science

(in Oceanography)

The Graduate School

The University of Maine

May 2024

Advisory Committee:

Margaret Estapa, Assistant Professor of Oceanography, Advisor

Lee Karp-Boss, Professor of Oceanography

Kara Lavender Law, Sea Education Association

UNIVERSITY OF MAINE GRADUATE SCHOOL LAND ACKNOWLEDGMENT

The University of Maine recognizes that it is located on Marsh Island in the homeland of Penobscot people, where issues of water and territorial rights, and encroachment upon sacred sites, are ongoing. Penobscot homeland is connected to the other Wabanaki Tribal Nations— the Passamaquoddy, Maliseet, and Micmac—through kinship, alliances, and diplomacy. The University also recognizes that the Penobscot Nation and the other Wabanaki Tribal Nations are distinct, sovereign, legal and political entities with their own powers of self-governance and self-determination.

UNIVERSITY OF MAINE DARLING MARINE CENTER LAND ACKNOWLEDGMENT

The Darling Marine Center recognizes that it is located in South Bristol along the Damariscotta River in the homeland of the Wabanaki Tribal Nations, where issues of water and territorial rights, and encroachment upon sacred sites, are ongoing. The historic Walinakiak Abenaki Tribe and other tribal peoples of the Pemaquid Peninsula area are connected to the modern, consolidated Abenaki Tribal Nation in Quebec and other Wabanaki Tribal Nations—the Passamaquoddy, Penobscot, Maliseet, and Micmac—through kinship, alliances, and diplomacy. The Darling Marine Center recognizes that the Wabanaki Tribal Nations are distinct, sovereign, legal and political entities with their own powers of self-governance and self-determination.

MESOPELAGIC MICROPLASTIC TRANSPORT INTERACTIONS WITH THE BIOLOGICAL CARBON PUMP

By

Mikayla Clark

Thesis Advisor: Dr. Margaret Estapa

An Abstract of the Thesis Presented in

Partial Fulfillment of the Requirements for the

Degree of Master of Science

(in Oceanography)

May 2024

Numerous studies on the transport and fate of plastic have alluded to a size-specific mechanism for removing microplastics (plastics below 5mm in diameter) from the epipelagic. Plastics like polyethylene and polypropylene which are less dense than seawater during manufacturing and use have been found throughout the water column and even in seafloor sediments. However, the mechanism for their vertical transport is poorly understood. This project calculates the vertical flux of microfibers during the 2021 EXPORTS North Atlantic campaign and captures the decline of the spring bloom from the base of the mixed layer to the mesopelagic by utilizing both lagrangian and semi-lagrangian sediment traps to capture sinking particles. In addition to creating a flux profile of both microfibers and particulate organic carbon, polyacrylamide gels were attached to the base of sediment trap tubes and used to visually observe the relationship between microfibers and organic aggregates. Laboratory experiments validated the use of gels in microfiber collection by showing that the density gradient of the gels

does not disaggregate fibers from marine snow and artificially made aggregates with polyester and polypropylene microfibers remain intact. The data shown by the gels demonstrate little correlation between microfibers and particulate organic carbon, which agrees with the flux profile comparisons. These new methods of microplastic collection for vertical flux measurements allow for direct visualization of plastic in organic particles which can aid to validate theories of the transport of plastic by the biological carbon pump.

DEDICATION

This thesis is dedicated to two wonderful individuals who passed away during its writing. It would not have been written without them. Dr. Thomas Aquinas Henry for supplying me with microscopes and textbooks for as long as I can remember and cultivating my love of science. And to William Clark for fostering my spirit of adventure and encouraging me to create my own path.

ACKNOWLEDGEMENTS

This research was funded by the NASA EXPORTS program, the University of Maine MARINE program, and the University of Maine School of Marine Sciences. Additionally, I would like to thank Colleen Durkin, Jeremy Rich, Sean O'Neill, Elizabeth Minor, Erik Hendrickson, and the Darling Marine Center hatchery team.

Table of Contents

LIST OF TABLES

LIST OF FIGURES

Chapter 1

A REVIEW OF MICROPLASTIC INTERACTIONS WITH THE BIOLOGICAL CARBON PUMP

1.1.Introduction

Plastics are persistent pollutants that have been exponentially increasing in their production since the 1980s (Kvale et al., 2020). The mismanagement of plastic waste is a significant cause of plastic pollution in the ocean. In the marine environment, studies show marine life may consume plastic and have adverse health effects (Law et al., 2010). These plastics are prone to fragmentation via physical, biological, and chemical degradation. Smaller plastics, primarily formed via fragmentation but also introduced into the environment via cosmetics such as microbeads (Law et al., 2010), are known as microplastics. Although the term "microplastic" is one used freely, there is no standard size range for plastics in this category. The most common definition for microplastics is a plastic particle less than 5mm in diameter (Law, 2017, Lenaker et al., 2019).

Microplastics are ubiquitous in the world's oceans (Cózar et al., 2014). Marine life such as coral, zooplankton (Cole et al., 2016), shellfish, and mesopelagic fish ingest microplastics either accidentally (via proximity to food) or actively (Rochman et al., 2015). An in-depth study found microplastics in the intestinal tracts of 25-28% of fish and 33% of shellfish sold at markets in the U.S. and Indonesia (Rochman et al., 2015). Provencher et al. (2018) and Davison & Asch (2011) respectively found that the standing stock of plastic within the stomachs of seabirds (Provencher et al., 2018) and mesopelagic fish (Davison & Asch, 2011) is within the same order of magnitude as the estimates of freely floating plastics in the ocean. In the environment, plastic is prone to chemical leaching which can decrease the photosynthetic efficiency of certain types

of algae (Liu et al., 2020) or introduce endocrine-disrupting chemicals into ecosystems (Chen et al., 2019). Additionally, microplastics function as transport vectors of persistent organic pollutants such as per- and polyfluoroalkyl substances (PFAS) to other ecosystems and into the food web (Bakir et al., 2016).

1.2. Where does the plastic go?

Tracking microplastics is imperative to understanding their ecosystem effects. Global models of microplastics in the marine environment significantly overestimate the amount of buoyant microplastic present in the surface ocean when compared to field sampling methods by several orders of magnitude (Kvale et al., 2020). This difference in recorded abundances may be due to size preferential sampling of net trawls as well as limited studies of plastics in the water column. Most plastic surveys in the ocean historically used 330μm mesh nets as the standard, missing all particles smaller than that threshold.

Other potentially understudied sinks of microplastics include nano-fragmentation, predation, biofouling, and shore deposition (Cózar et al., 2014). Erikson et al. (2014) expected to find higher quantities of microplastics than macroplastic at the surface during their survey, as the primary source of microplastics is fragmentation from larger macroplastics. They found that the opposite was true at nearly all sites. In addition, Cózar et al. (2014) found that when plastic size reached below 5mm, there were fewer plastics collected than theoretical models had predicted.2. These observational studies may suggest a size-specific process of microplastic removal from the surface ocean that is yet to be thoroughly described (Cózar et al., 2014, Erikson et al., 2014).

An in-depth look at the vertical plastic profile beneath the surface of the North Pacific subtropical Gyre (Egger et al., 2020) showed that most fragments found at depth were sourced

from initially buoyant plastics accumulating at the surface. Both the vertical MOCNESS (Multiple Opening/Closing Net and Environmental Sensing System) tows and the horizontal Manta net trawls found most of their samples were made of polyethylene and polypropylene which are both buoyant in seawater (Egger et al., 2020). Finding these types of buoyant plastics at depth is far from uncommon. Polyethylene and polypropylene dominated a depth-resolved study in the North Atlantic Ocean as well. Pabortsava & Lampitt (2020) found that polyethylene, polypropylene, and polystyrene each distributed from the surface to the mesopelagic, despite polystyrene being the only material of the three to be negatively buoyant in seawater. Additionally, this study found that the mass of plastic was distributed among all latitudes in the Atlantic Ocean, despite the Southern Hemisphere having a significantly lower input of plastic from coasts. This indicates that plastic may circulate between oceans at an even greater rate than previously expected, primarily driven by surface currents and atmospheric deposition.

Models incorporating mesoscale physical processes into microplastic dispersal models have shown that wind, stratification, and geostrophic currents all play a role in both the vertical and horizontal movement of microplastics (Chevalier et al., 2023). Wind-driven mixing can force buoyant microplastics deeper into the water column. Additionally, the modeling study conducted by Chevalier et al. (2023) showed an impact of seasonal mixing on the vertical distribution of plastics. In the summer months, few microplastics were found deeper than 20 meters due to heavy stratification and lower wind stress. The winter months and the onset of seasonal mixing was shown to distribute neutrally buoyant microplastics uniformly throughout the water column. Studies of microplastic accumulations in mesoscale eddies also suggest that buoyant microplastics may be distributed throughout the water column due to geostrophic currents (Vega-

Moreno et al., 2021). Although we know of the prevalence of buoyant microplastics at depth in all areas of the world's oceans, the mechanisms of their transport are still largely unknown.

To further complicate understanding of the transport of microplastics, studies have shown that the shape of the particle affects sinking velocity more than the particle density (Khatmullina & Isachenko, 2017). The three most common shapes of microplastics found in the environment are microbeads, fragments, and fibers. While they have relatively low natural abundance, microbeads are used to measure sinking velocities for various plastics such as in the experiment conducted by Cole et al. (2016). The irregular, non-spherical shapes of fragments and fibers make it difficult to use the same techniques to model their sinking velocities. Physical mixing processes influence the motion of each shape of plastic differently and that is apparent in their depth-resolved abundances.

Studies of plastic fibers have found them similarly distributed at all depths, regardless of polymer type (Lenaker et al., 2019) and fibers constitute the majority of microplastics found in deep-sea sediments (Law et al., 2010). This finding is inconsistent with observations that fibers or fishing line cuts have a significantly lower settling velocity than fragments or spheres (Khatmullina & Isachenko, 2017). Settling velocities for fibers are estimated to decrease with an increase in size due to an increase in the amount of drag experienced in proportion to the fiber's density (Khatmullina & Isachenko, 2017). Looking at sinking velocity measurements alone, negatively buoyant, spherical, and fragments are expected to encompass the majority of plastic at depth whereas fibers, which have a lower sinking velocity, are expected to be more abundant at the surface (Khatmullina & Isachenko, 2017). Observational studies show that the distribution in the environment varies significantly (Lenaker et al., 2019). Fibers have been noted in numerous studies to be found almost uniformly throughout the water column (Lenaker et al., 2019). This

indicates that additional processes exist which affect the distribution of plastic more than their material densities.

1.3. Plastics and the Biological Carbon Pump

While hydrodynamics and wind mixing are known to play a role in plastic transport in the surface ocean, the biological carbon pump (BCP) is thought to be a key factor in vertical microplastic transport at depth. The BCP is a mechanism that transports carbon and organic material from the surface to the deep ocean most commonly in the form of marine snow and zooplankton fecal pellets (Durkin et al., 2021). The efficiency of the BCP is often quantified by measuring the vertical flux of particulate organic carbon (POC), predominantly in the form of aggregates, from the surface ocean to the deep sea and sediments. To accurately model the biological carbon pump's role in the transportation of microplastics, it is important to study and compare the flux of POC and the flux of microplastics. POC is transported due to several mechanisms, most of which also transport microplastics. The three most-studied pathways are biofouling, aggregation into marine snow, and egestion as fecal pellets.

1.3.1. Biofouling

Biofouling is the buildup of organisms and organic material on a (typically anthropogenic) surface over time. This process is stimulated by the hydrophobic properties of plastic and is thought to cause sinking via an increase in density due to the colonization of microscopic organisms (Kaiser et al., 2017). A study by Kaiser et al. (2017) showed that in estuarine, coastal, and Atlantic waters, biofouling was unable to cause polyethylene to sink during the 14 weeks of their experiment. However, biofouling increased the sinking velocity of the already negatively buoyant polystyrene by 28% in Atlantic waters. While the development of

a biofilm alone failed to cause polyethylene to sink, the attachment of mussel larvae causes the plastic to become negatively buoyant (Kaiser et al., 2017).

Sinking rates of polyethylene were positively correlated with the number of mussel larvae attached to the polyethylene fragment (Kaiser et al., 2017). Mussels use 20 µm threads to attach to a surface, making them one of the few organisms that may be able to settle on microplastics. This also implies a lower limit to the size of particles that can be sunk via invertebrate settling. An additional theory is that some small plastic particles may sink faster than a significant biofilm can form (Kaiser et al., 2017). In addition to increasing the sinking velocity of plastic particles, the development of a substantial biofilm may also be able to impact the transport of organic carbon to the deep sea or sediments. The transportation of microplastics with biofilms on their surface is harder to predict than unfouled microplastics (Gaylarde et al., 2023). The behavior of these contaminants becomes similar to biological material and thus changes based on the surrounding environment.

1.3.2. Marine Snow

Another mechanism that may be responsible for the transport of positively buoyant plastic to depth is the aggregation of plastic into sinking phytoplankton aggregates. Phytoplankton secrete polysaccharides that have relatively high stickiness (Passow, 2002). Transparent exopolymers (TEP) are a specific type of polysaccharide stainable with Alcian Blue and produced in part by senescing phytoplankton, particularly diatoms (Passow, 2002). These particles, while neutrally buoyant on their own, are sticky and promote the aggregation of marine snow. In areas of high primary productivity and higher TEP concentrations, plastic is thought to also be aggregated into sinking marine snow (Galgani et al., 2022). To test the aggregation of plastic into phytoplankton aggregates, Long et al. (2015) combined microbeads and two types of

phytoplankton into flow-through tanks. Microbeads readily aggregated into both samples, although more permeable and fragile aggregates incorporated more than those high in TEP particles due to the higher surface areas. Regardless of TEP concentration, lab experiments show microplastics are found to be incorporated into phytoplankton aggregates.

Modeling studies such as the one conducted by Yoshitake et al. (2023) have worked to quantify the settling velocities of microplastics adsorbed to phytoplankton aggregates. This study's findings showed that modeled aggregates containing microplastics sank from the surface to one hundred meters depth by day four of the study. In this model, the settling velocity was mainly influenced by the size of the particles rather than their density. The authors noted that this settling speed may decrease if the buoyancy of the plastics incorporated into the aggregates outweighed the increase in velocity due to an increased size. The disaggregation and resuspension of aggregates at depth was not included in this model but may be a critical component of the vertical transport of plastic in the environment.

1.3.3. Fecal Pellets

Perhaps the most efficient transport mechanism the biological carbon pump offers is the inclusion of microplastics in zooplankton fecal pellets. While zooplankton are preferential feeders, studies show that zooplankton readily feed upon microplastics (Cole et al., 2016). This causes the plastic to be internally repackaged with natural material and released in the form of fecal pellets (Cole et al., 2016). Fecal pellets are likely one of the primary vectors of carbon transport to the deep ocean (Durkin et al., 2021). The inclusion of plastic into this process is not found to lower the size of the pellets or the egestion rates of zooplankton (Cole et al., 2016), indicating that the repackaging of plastics into pellets may rapidly increase plastic sinking velocity and therefore overall plastic transport to the deep ocean.

1.4. Plastic Affects the BCP

Several studies mentioned thus far have shown the biological carbon pump as a possible mechanism for plastic transport. With this mechanism, it is assumed that the vertical flux of plastic varies linearly with the flux of organic material. Newly conducted depth-resolved studies indicate that this comparison is not as direct as theoretically assumed. While Galgani et al. (2022) found that plastic flux by mass did correlate with the flux of POC, the relationship was less correlated than the relationship between biological particles such as TEP and Coomassie stainable particles (CSP). Additionally, this study found that most plastic samples below 300 m were free from biofilms. This could likely be due to disaggregation once the particle reaches depths that are inhospitable to the colonized organisms. The study by Galgani et al. (2022) also showed a higher accumulation of microplastics in areas of higher primary productivity, deduced from measurements of chlorophyll a. The highest plastic mass in this study was found between 100 -150 m depth, which correlated to an increase in chlorophyll a, TEP particles, and particulate organic carbon (Galgani et al., 2022).

While the biological carbon pump may influence plastic transport, plastic may also influence carbon transport. The consumption of plastics can lower the overall reproductive potential and growth rates of zooplankton (Cole et al., 2016). As zooplankton fecal pellets, as well as their sinking carcasses and molts, are major transports of carbon (Steinberg & Landry, 2017), a reduced reproductive potential may lower global carbon export. Additionally, plastic has been shown to alter the physical properties of sinking aggregates. In a laboratory setting with high quantities of microplastics, Cole et al. (2016) found that the incorporation of microplastics into copepod *C. helgolandicus* fecal pellets decreased the overall density and sinking velocityCole et al. (2016) also found that several of the egested beads were free-floating,

prompting a comparison of whole fecal pellets and partial fecal pellets in the plastic versus control studies. They found that when plastic was incorporated into aggregates, there were larger numbers of partial fecal pellets compared to whole pellets. This has several important implications. Partial pellets have a lower sinking velocity, and this breakage can cause disaggregation. The presence of partial fecal pellets is likely to be made more common with the inclusion of plastic due to less organic material being available to bind. Plastics also are suspected to disrupt the peritrophic membranes which aid in holding fecal pellets together (Cole et al., 2016). Disruption of these membranes makes particles more likely to disaggregate. Disaggregation prompts the early release of both plastic and particulate carbon into the water column before it can be sequestered in the ocean sediments. This process keeps both carbon and plastic in the water column, limiting future carbon uptake and keeping plastic accessible to marine life.

The BCP is not immune to alteration from the inclusion of plastic. Plastics have been shown to slow sinking rates of aggregates and promote disaggregation which both ultimately lowers the rate of carbon sequestration and resuspends plastics and organic matter into the water column (Cole et al., 2016). Further field-based research is needed in this area as the majority of microplastic sinking velocity measurements have been conducted in laboratories using microbeads. A limit on depth-resolved studies of microplastics makes it difficult to elucidate the actual transport mechanisms of buoyant plastics. The biological carbon pump may be a successful mechanism for the transport of plastic to depth, but the incorporation of less buoyant particles may slow the overall rate of carbon sequestration and plastics in the marine food web.

CHAPTER 2

OBSERVATIONAL STUDY OF MICROPLASTIC TRANSPORT DURING THE NORTH ATLANTIC SPRING BLOOM: INSIGHTS FROM THE EXPORTS CAMPAIGN

2.1. Introduction

There are few studies of microplastics in the mesopelagic and understanding the relationship between carbon and plastic transport aids in modeling plastic concentrations and fate throughout the ocean rather than only at the surface. Our observational study occurred in May 2021 as a part of the EXport Processes in the Ocean from RemoTe Sensing (EXPORTS) campaign in the North Atlantic. This campaign aimed to quantify the biological carbon pump (BCP) during the senescence of the annual spring phytoplankton bloom. The objective of this study was to identify if the BCP plays a part in the vertical transport of microplastics.

All sampling was done in the center of an anti-cyclonic, retentive, mesoscale eddy (Johnson et al., 2023). Modeling studies have shown that anti-cyclonic eddies have the potential to accumulate microplastics within them and could accumulate up to 9 times as many microplastics as cyclonic gyres (Brach et al., 2018). However, there are few observational studies of microplastics within anti-cyclonic eddies to verify models of microplastic transport in these regions. Johnson et al. (2024) identified the water between the mixed layer and 200 m as the surface eddy core waters (SCW). During our sampling period, this region was heavily stratified. The well-mixed regions below the SCW within the eddy core were called eddy core waters (ECW). Our samples were collected primarily from the ECW, although several depths were sampled within the SCW, just below the mixed layer.

Several storm events marked the separation between sampling periods, known throughout this paper as “epochs” (Table 2.1), which promoted mixing in the SCW and an overall weakening of stratification during these events. High winds are known to mix microplastics deeper into the water column, although strong stratification may dampen the effects of this process (Chevalier et al., 2023).

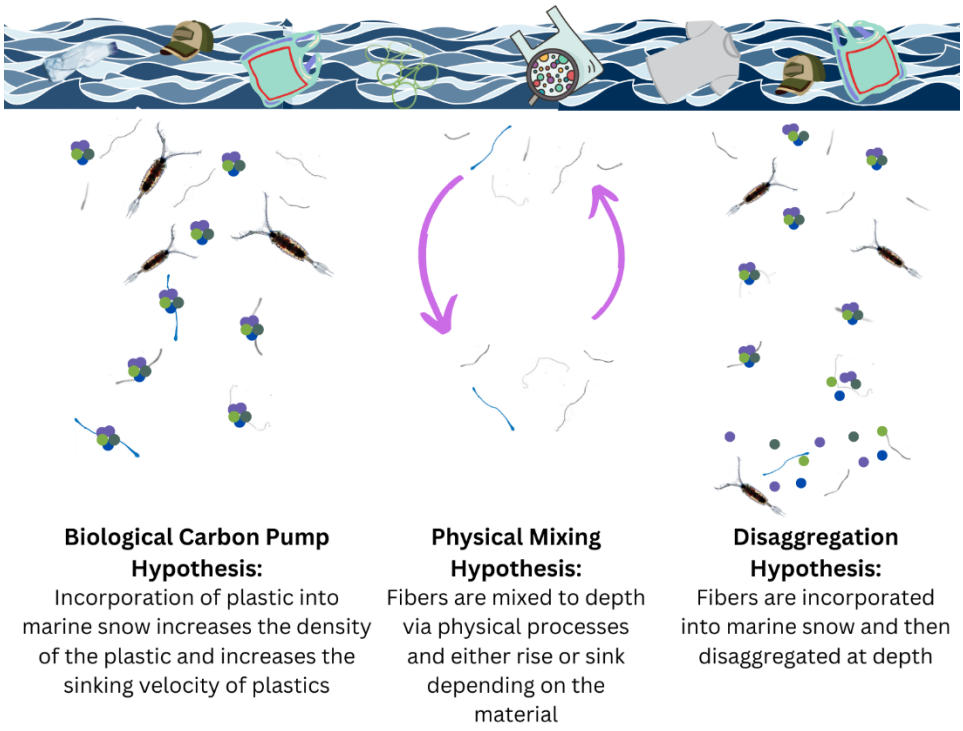

Figure 1: The figure shows three likely hypotheses for the vertical transportation of plastic fibers. From left to right, these hypotheses are the biological carbon pump hypothesis (plastic is transported with marine snow), the physical mixing hypothesis (plastic is transported independently and may rise, sink, or remain neutrally buoyant depending on the particle), and the disaggregation hypothesis (plastic is transported with marine snow to a certain depth and is resuspended as aggregates are remineralized).

The hypotheses behind the vertical transportation of plastic fibers are shown in Figure 1. The biological carbon pump hypothesis posits that there is a direct relationship between carbon flux and the flux of anthropogenic fibers because the plastic is transported by marine snow. What we have coined as the "disaggregation hypothesis" allows for the initial transportation of fibers with marine snow, but fibers are then disaggregated at depth due to zooplankton feeding, or other remineralization processes. The hypothesis of physical mixing considers that microplastics are drawn into the water column due to strong wind-induced mixing or other processes and either continue to sink or become "trapped" by strong density gradients formed during restratification after the wind event (Chevalier et al., 2023).

Our sample collection methods allow for the comparison of carbon flux and the flux of anthropogenic fibers which allows us to determine which of these processes is affecting the distribution of our samples. Sediment traps allow for the isolation of sinking particles, unlike manta trawls or the bulk filtering of water using vacuum pumps, which makes them a unique tool for identifying sinking microplastics in the ocean. Identifying the driver of vertical plastic transport can better aid in modeling the fate of microplastic pollution.

2.2. Methods

2.2.1. Sample Collection

Samples were collected on board the RRS James Cook as a part of the EXPORTS 2021 field campaign during the end of the North Atlantic spring bloom. Two types of sediment traps were deployed to capture the flux of carbon and other materials to the mesopelagic. Five surface tethered traps (STTs) were deployed at 75 m, 125 m, 175 m, 330 m, and 500 m for the first two epochs and were deployed at 145 m, 195 m, 330 m, and 500 m for the third epoch when the

estimated mixed layer depth increased (Table 2.1). These traps are attached to a buoy at the surface and collect sinking particles while drifting along with the current. Two neutrally buoyant sediment traps (NBSTs) (Estapa et al., 2020) operated at 177 m and 178 m during the first epoch, although the one set at 178 m spent a large amount of time outside of its programmed depth and has been excluded from this data set. Neutrally buoyant sediment traps are not attached to a surface buoy and make active buoyancy adjustments to maintain a preprogrammed depth. These traps have the added benefit of being unaffected by shear caused by differing current velocities at the surface and trap depths (Estapa et al., 2020). Five NBSTs operated during the third epoch at depths of 109 m, 143 m, 199 m, 330 m, and 502 m. All sampling events are summarized in Table 2.1 and sampling procedures were similar to Estapa et al. (2021).

Table 2.1: A list of trap types and dates for each epoch.

Epoch	Dates in 2021	Trap Types (# Deployed)	Depths Targeted (m)
1	05-07 May	STT (5), NBST(1)	75, 125, 175, 330, 500*
2	12-15 May	STT(5)	75, 125, 175, 330, 500
3	22-25 May	STT (5), NBST (5)	100**, 145**, 195**, 330, 500

* The polyacrylamide gel sample from this depth was lost during collection.

** The depths targeted during epoch 3 were changed to reflect the deepening mixed layer during this time.

Each trap consisted of four tubes, two carrying 500 mL of 70 ppt salinity, 0.1% formaldehyde-poisoned brine overlain by 1 µm filtered surface seawater, one dedicated to genetic sequencing (not discussed further here), and one carrying a polyacrylamide gel overlain with filtered surface seawater. This setup is further described by Durkin et al. (2023). For our samples, we utilized the brine tubes to collect what will further be referred to as “bulk fibers” and the polyacrylamide gel collector. After sampling, bulk fibers were collected by passing the

brine tube contents through a 335 μm screen and manually removing fibers from the screen with forceps under 7x magnification. Fibers from a single sediment trap depth were rinsed off forceps into a conical tube of pure water, whose contents were then transferred onto a 1 μm polycarbonate membrane filter (Nuclepore) under low vacuum and dried at sea in a HEPA-filtered flow bench and stored dry until analysis. Gels were stored at −17 °C until 24 hours before imaging when they were thawed at 4 °C.

The field collection of fibers was conducted opportunistically at sea and the complete isolation of samples from plastic contamination was not possible. However, field and laboratory blanks were collected during all steps described above and imaged for contamination. Field blank gels were collected on the sediment trap array and treated exactly as the collected field samples. During processing and imaging, blank filters were placed on the lab bench beside the gels and then imaged to account for any error in the laboratory setting. On shore, all sample handling was done while wearing closed, pure cotton laboratory coats and purple nitrile gloves.

2.2.2 Gel Trap Fiber Collection

Particles within gel traps were identified as potential plastic fibers based on the following criteria: highly saturated color, smooth sides with frayed ends or evidence of fraying throughout, fiber-like morphology, and an opaque appearance. Examples of this classification method are shown in Figure 2. Fibers were imaged 2-3 times each in the polyacrylamide gel collector using an Olympus SZX2 microscope with a Teledyne Lumenera Infinity camera attachment. The microscope was set to 20x, 65x, or 125x magnification depending on the size of the fiber.

A. 

B. 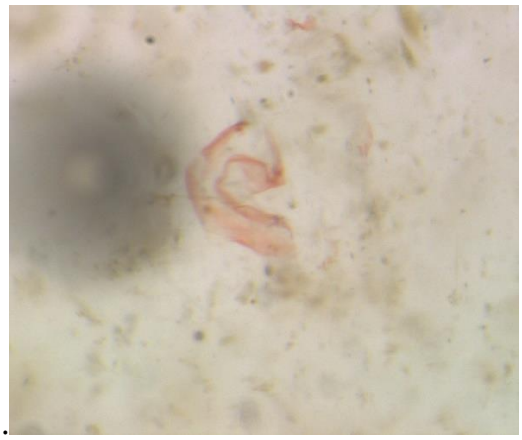

Figure 2: Images from polyacrylamide gel collector. Image A shows a particle classified as a fiber due to the high saturation, opaqueness, and evidence of fraying. Image B shows a particle that is highly saturated but does not fit the qualifications due to its transparency and morphology. The 1 mm scale bar is the same for both images.

In addition to size, each fiber's color and any association with organic material were recorded. This association was determined by whether a fiber had organic material attached to it, regardless of the size of the organic material relative to the fiber. Examples of these classifications are shown in Figure 3.

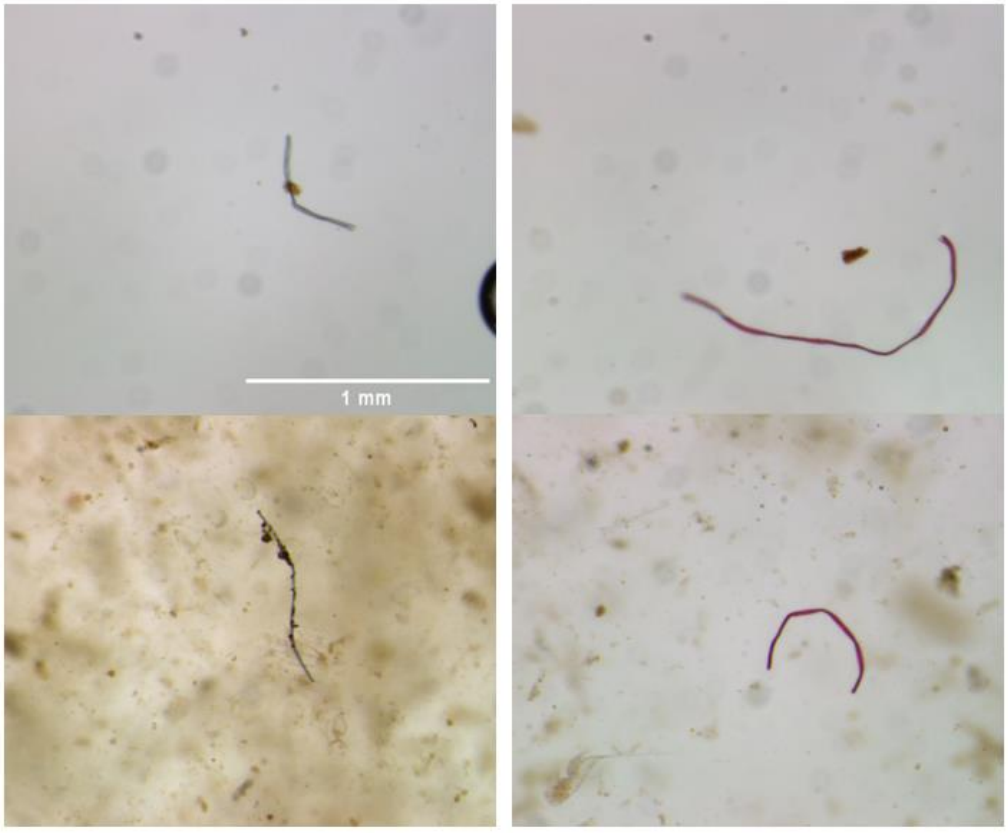

Figure 3: A visual description of how organic matter association was determined. Images on the left show fibers that were classified as being associated with organic matter. Images on the right show fibers that were classified as not being associated with organic matter. The 1 mm scale bar is the same for all images.

2.2.3. Bulk Filtered Fiber Collection

Bulk fibers were hand-picked off 330 μm screens on the ship under magnification and placed onto 25 mm diameter, pre-weighed, 1 μm pore size polycarbonate membranes (Nuclepore) as described above. These fibers were used in the polymer composition analyses detailed in Chapter 3. The filters containing bulk fibers were imaged alongside laboratory blanks to account for any potential contamination. On shore, fibers were manually removed from the

remaining organic matter on the filters and placed onto another set of pre-weighed 1 μm pore size Nuclepore membranes. These filters were dried in a plastic-clean oven alongside a set of three blank filters and then weighed on a microbalance (Mettler-Toledo WXTE) to determine the mass of fibers to the nearest 0.001 mg. Following this procedure, each fiber was removed and placed into a glass-bottomed 24-well plate for individual imaging and sizing. Any remaining organic matter was dissolved using 0.5 mL of 33% hydrogen peroxide which was allowed to evaporate completely over 48 hours before rinsing with MilliQ. Bulk fibers were used for the determination of fiber composition which is described in Chapter 3.

An average of 2.2 fibers were found on blank filters exposed to ambient laboratory conditions during analysis. One field blank filter contained a tangle of frayed yellow fibers which was discounted as it matched the color and structure of the rope used for deployment. No other samples from bulk or gel traps contained this type of fiber. The singular fragment found in the samples was discounted from analysis due to it being of similar appearance to the collection tubes.

2.2.4. Fiber Measurements

All fiber images were processed and sized using a thresholding code that separates the fiber from its background and finds the area in pixels. Fibers were identified using a simple threshold difference from the background, and then they were sized using the MATLAB function “bwconncomp” which returns the geometric properties of particles in binary images. The output of this function is shown in Figure 4. The area of each fiber was determined using a known pixel: area ratio. This pixel: area ratio was determined using a 5 mm scale imaged beneath the same microscope at all levels of magnification. To quality control the code and determine its accuracy,

a subset of the fibers was manually measured using ImageJ software to find the length and width. Several of these measurements were taken multiple times and compared to the automated measurements to determine error, and a +/- 5% error was applied to all measurements.

Figure 4: A sample image showing the thresholding program's output after background removal. The fiber is easily identifiable against the black background. The scale bar is 500 µm or 0.5 mm.

2.2.5. Blank Fiber Volume Corrections

An average of 14 microfibers with a total volume of 0.05 mm^3 were found on each gel blank. The average blank fiber volume (V_B, mm^3) was subtracted from the fiber volume in each sample (σV_i, mm^3) prior to calculation of the blank corrected volume flux (F_T, $mm^3\ m^{-2}\ d^{-1}$) by normalizing to trap collection area (A, m^2) and deployment elapsed time (t, d^{-1}). This way, variations in sizes with depth and trap type were accounted for. Trap deployment durations have been published in Estapa et al. (2023). The following equation was used:

Equation 1:

$$F_T = \frac{(\sum V_i) - V_B}{A \times t}$$

For fibers in the polyacrylamide gel collectors, the flux was determined volumetrically in units of $mm^3\ m^{-2}\ d^{-1}$ rather than in the more standard mg $m^{-2}\ d^{-1}$. The volume was calculated by using the average width of the fibers and the assumption that the fibers had circular cross sections (width = depth). Additionally, a subset of the fibers characterized in gels were later manually removed and used for sinking speed measurements described in Chapter 3.

2.3. Results

2.3.1. Size Distribution of Microplastics in the Water Column

Understanding the size distribution of sinking microplastics throughout the water column is important for modeling their transport and fate. Vertical variations in size distribution can be affected by settling velocities, interactions with biota (i.e. being eaten and egested due to zooplankton feeding on aggregates), and the formation of biofilms. Several studies have identified a gap below 5 mm in the size distribution of plastics collected at the surface, alluding to a size-specific mechanism of microplastic transport in the water column (Erikson et al., 2014; Cózar et al., 2014).

In our study, we examined the size distribution of fibers for trends with both depth and time. The average size of fibers did not vary significantly between epochs 1 and 3 in both the polyacrylamide gel and bulk samples. Fiber sizes from epoch 2, however, were significantly smaller than the other two epochs for both sampling methods (t-test, $p < 0.001$). In epoch 3 NBSTs collected larger fibers than their STT counterparts at the same depths (t-test, $p < 0.001$),

although there were no significant differences found between fiber sizes in epoch 1 NBSTs and STTs. Additionally, the size did not vary significantly with depth (Figure 5). Fibers less than 1 μm^3 in volume were 24.8 times more abundant than fibers greater than this volume. Most of the larger fibers were found in epochs 1 and 3, with the largest fibers being found in epoch 1.

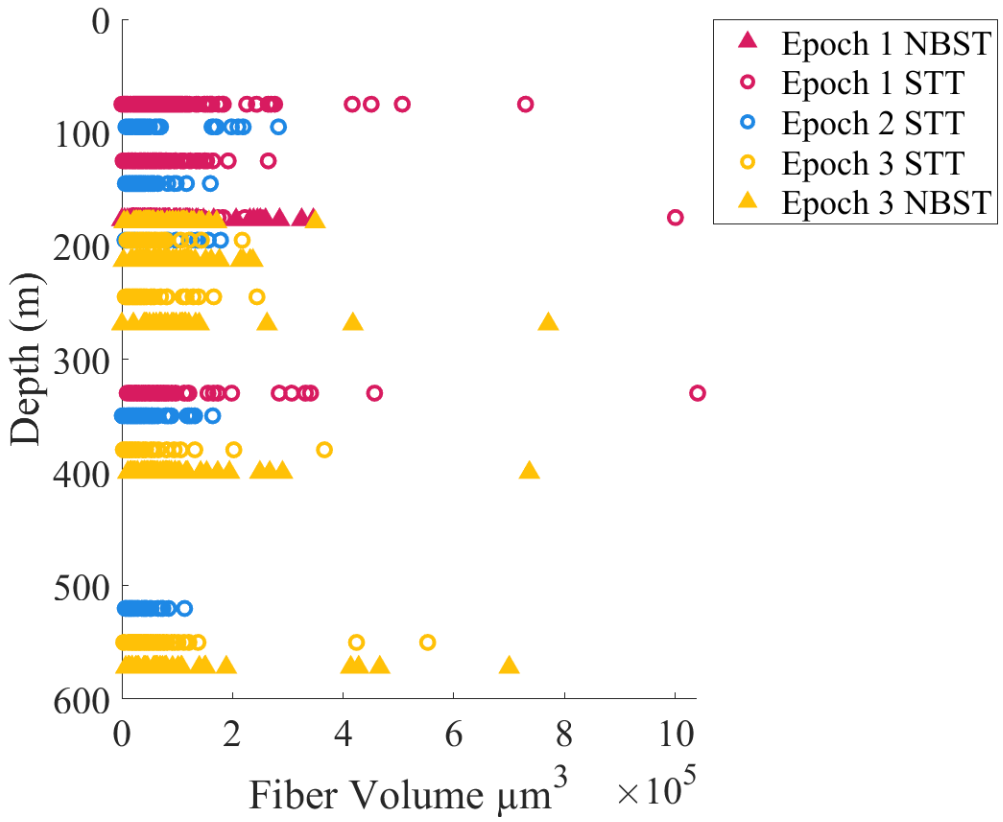

Figure 5: Size distribution of fibers collected in polyacrylamide gel traps by depth. The average volume of fibers collected throughout all three epochs does not change significantly with depth. Each symbol represents a single fiber. The average volume of fibers found in epoch 2 (blue) was significantly smaller than in epochs 1 and 3. The depths were slightly offset for visibility.

2.3.2 Flux of Fibers in the Water Column

2.3.2.1. Bulk Mass and Numerical Flux of Fibers

The mass of fibers in total was small compared to the estimated uncertainties shown in Table 2.2. The average mass of fibers on filters was 0.033 mg with an average relative uncertainty of approximately 20%. There was no trend in mass with depth for bulk fibers collected in either epoch or trap type. Overall fewer fibers were found in epoch 2. Average area, volume, and length did not significantly change in bulk samples between epochs. Neutrally buoyant sediment traps overall collected fewer fibers, except for the NBST at 330 m. The mean area, volume, length, and mass of fibers in the bulk samples across each trap are shown in Table 2.2. Uncertainty was determined using both material and filter mass measurements.

Table 2.2: Physical characteristics of the bulk fibers showing the trap type, mean area, volume, and length of fibers, as well as the total mass flux of fibers on the filters and the uncertainty.

Depth	Trap Type	Mean Area (mm^2)	Mean Volume (mm^3)	Mean Length (mm)	Total Mass Flux ($mg\ m^{-2}\ d^{-1}$)	Mass Flux Uncertainty ($mg\ m^{-2}\ d^{-1}$)
75	E2 STT	0.00175	0.00552	3.82	0.764	0.0574
125	E2 STT	0.00284	0.00407	1.68	0.860	0.1056
175	E2 STT	0.00170	0.00304	2.60	1.963	0.1191
330	E2 STT	0.00135	0.00236	1.64	0.955	0.1133
500	E2 STT	0.00152	0.00253	1.74	0.571	0.0687
95	E3 STT	0.00289	0.00576	2.03	1.329	0.0371
145	E3 STT	0.00144	0.00237	1.70	1.669	0.0782
195	E3 STT	0.00194	0.00466	2.86	2.593	0.1753
330	E3 STT	0.00142	0.00282	2.25	2.058	0.1123
500	E3 STT	0.00195	0.00474	2.80	3.547	0.0627
109	E3 NBST	0.00980	0.03173	2.29	2.482	0.0973

Table 2.2: Continued

143	E3 NBST	0.00256	0.01716	5.91	0.393	1.4405
199	E3 NBST	0.00164	0.00513	4.03	1.029	0.0575
330	E3 NBST	0.00195	0.00428	2.41	0.569	0.1506

We compared the mass flux of fibers to the total mass flux found in the sediment traps from these two epochs. On average, the fiber flux was 2 orders of magnitude lower than the total mass flux. Figure 6 shows large uncertainties in measuring the mass of fibers, which includes uncertainty from both measuring the filters before sampling and measuring the sample weights. There is no variation in depth and no significant variation between epochs 2 and 3 (t-test, $p > 0.5$). There is also no evidence of variation in fiber flux with the total mass flux, although the error is too high to determine this conclusively.

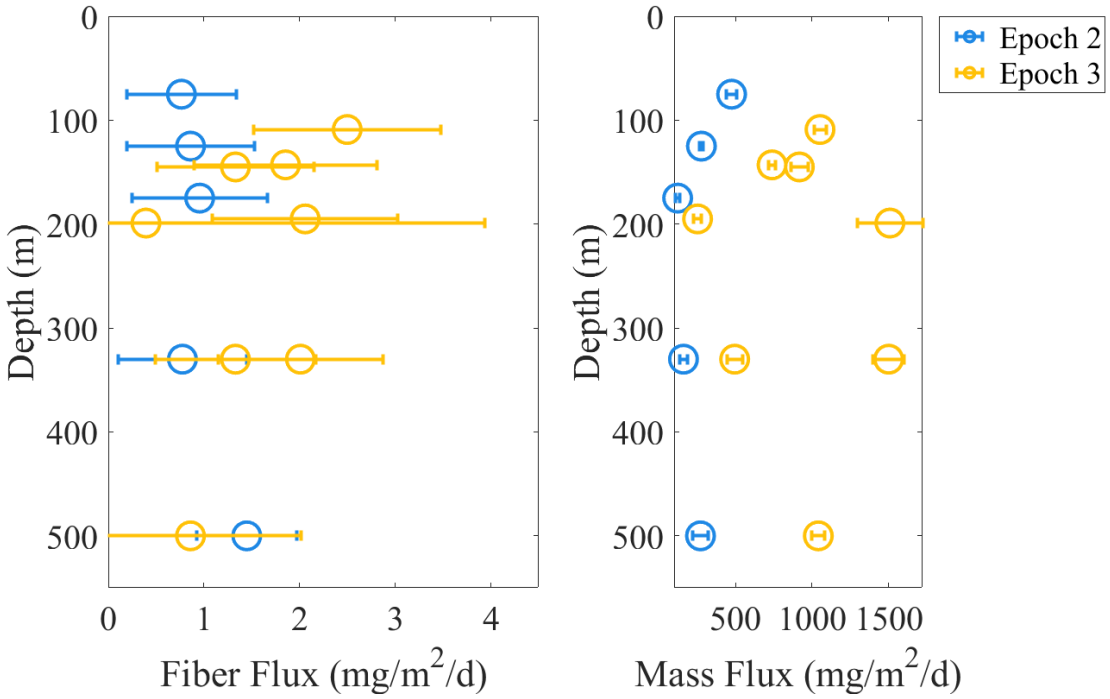

Figure 6: Mass flux of bulk-filtered fibers. Epoch 2 is shown in blue and epoch 3 is shown in gold. The figure on the left shows the mass flux of fibers with no significant depth trend. The figure on the right shows the bulk mass flux with an exponential decay in epoch 2 and no significant depth trend in epoch 3.

2.3.2.2. Volumetric Flux of Fibers

There was no variation in the average volume of fibers with trap type. Figure 7 shows no significant variation in fiber volume flux with depth (t-test, $p > 0.5$). Epoch 2 had a lower overall flux of fibers compared to epochs 1 and 3. There are differences between the volume of fibers collected between NBSTs and STTs at the same depths for three of the five pairs as shown in Figure 7. This difference is largest at 500 m during epoch 3 where the STT collected double the NBST flux at the same depth during the same deployment. Specific traps had large

disagreements between the NBSTs and STTs at the same depth, although the differences are inconsistent. This can be partially attributed to the patchiness of fibers in the water column.

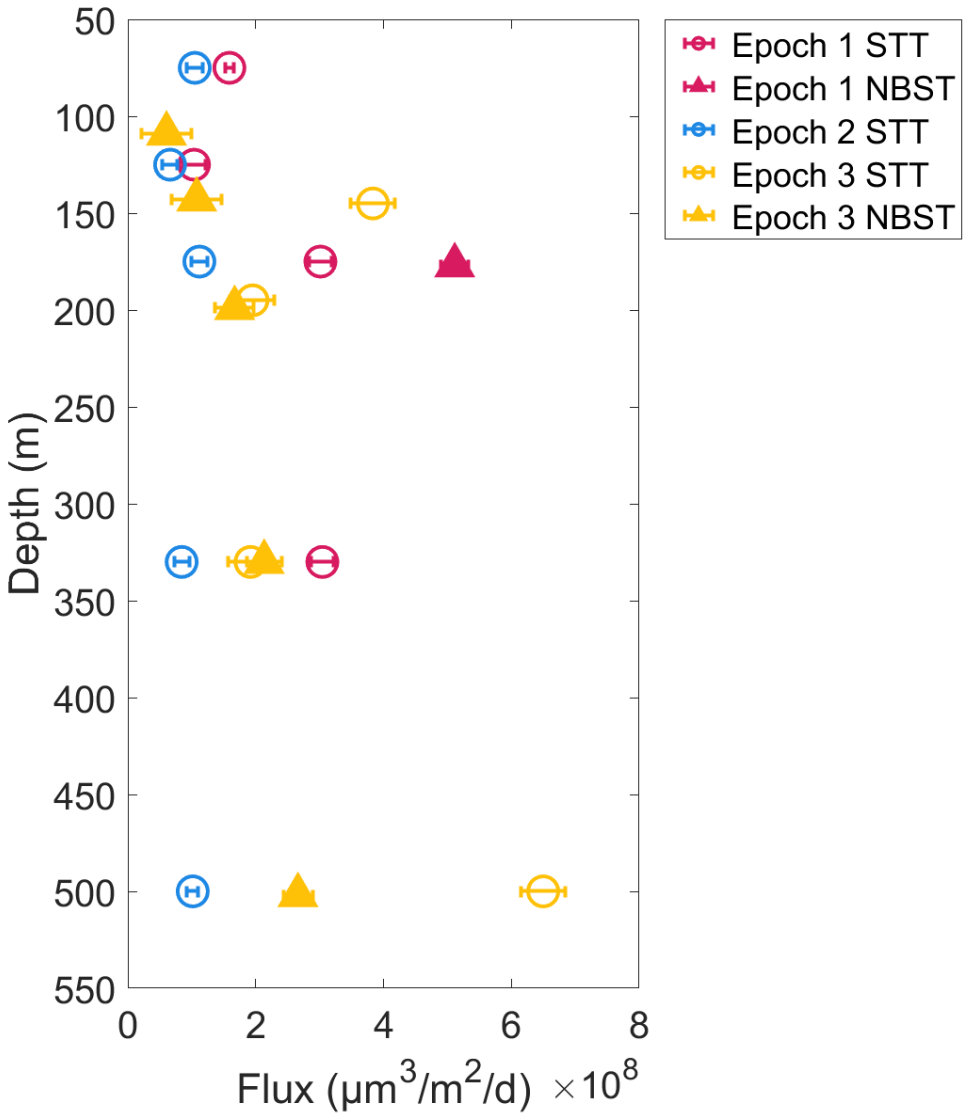

Figure 7: Volumetric flux of fibers measured in $\mu m^3\ m^{-2}\ d^{-1}$. The figure shows no consistent trend in depth, although the flux of fibers is lower in epoch 2 (blue). There are substantial differences between fibers collected in different trap types at three of the five duplicate depths: 144, 177, and 500 m.

2.3.3. Organic Matter Association

Between 2.4 and 17.7 % of the fibers (n = 1414) at depth had attached organic matter (Table 2.3). Laboratory experiments (detailed in Chapter 3), showed that gels retained fibers and attached aggregates under a variety of conditions, indicating that the gels did not cause the lack of attached organic material. The fraction of fibers with organic material attached is summarized in Table 2.3. Epoch 2 had a considerably lower number of fibers with organic material attached, despite POC flux being similar to epoch 1. Longer fibers were more likely to have organic material on them. Organic matter association with fibers did not vary significantly with depth or POC flux (t-test, $p > 0.5$). Organic matter attachment in general was extremely low throughout all epochs, but particularly epoch 2.

Table 2.3: A summary of fibers collected with organic matter.

Epoch	Total Collected Fibers	% Fibers with Organic Material
1	642	10.43
2	286	2.45
3	486	17.70

2.4. Discussion

The lack of variation in fiber size with depth suggests that if a size-specific mechanism is responsible for the transportation of these fibers into the water column, it occurs above the mixed layer depth. Our results also suggest no size-specificity in processes that would cause fibers to stop sinking (e.g. fragmentation). Previous studies of vertical fiber distribution in the water column also show no trend in fiber size with depth in the water column (Lenaker et al., 2019; Galgani et al., 2022). Additionally, the number of small fibers (less than 1 mm^3) was over 20

times the number of fibers larger than this size. While there was no depth trend in the ratio of small: larger fibers, the prevalence of smaller fibers is consistent with fibers being mechanically weathered over time.

The effects of the three large storms on the eddy throughout our sampling are detailed in Johnson et al. (2023). Notably, they weakened the stratification of the SCW. Previous literature has identified the base of the mixed layer as an area of plastic accumulation (Choy et al., 2019; Galgani et al., 2022; Uurasjärvi et al., 2021). In highly stratified environments, plastics which are only slightly denser than water in the mixed layer may become neutrally buoyant entering the pycnocline (Uurasjärvi et al., 2021). However, there was no significant accumulation in this area shown in our sampling between the SCW and the ECW. In settling tests described in Chapter 3, our fibers were found to be negatively buoyant at density equivalent of 330 m, so it is unlikely that our samples would accumulate at the base of the mixed layer.

Additionally, the type of sediment traps used for collection impacts the size of fibers sampled which should be considered in future microplastic sediment trap collection studies. As NBSTs are self-ballasting rather than being attached to a surface buoy, they have less disruptive effects caused by horizontal flow across the trap mouth (Estapa et al., 2021). The minimization of these effects allows for a more accurate separation of sinking and nonsinking particles. In epoch 3 the relative horizontal flow measured at the 500 m trap was 30 cm sec^{-1} which is above a threshold where effects may be observed on trap collection (Estapa unpublished data; Buesseler et al., 2007). The increased horizontal flow over the STT collection tubes may have caused smaller fibers to be preferentially trapped as larger fibers have a greater surface area for the current's force to affect.

There was no trend in mass with depth for bulk fibers and with data from gel traps collected in either epoch or trap type. This is consistent with findings in other literature (Galgani et al., 2022). The mass flux of the bulk samples is several orders of magnitude lower than the bulk mass of sinking POC material in the water column, indicating that the mass of fibers is not large enough to have an impact on total POC mass flux. The carbon: mass ratio of polyethylene (C_2H_4), a common plastic utilized in packaging is 0.86. If all our bulk fibers were polyethylene, the carbon flux from plastic would be 0.42 mg m^{-2} d^{-1}. This is three orders of magnitude smaller than our measured bulk fluxes and is likely negligible in our bulk carbon measurements.

As mentioned throughout this paper, the flux of POC decreased with depth as expected for biological material. Flux was highest in epoch 3 and similar between epochs 1 and 2. To further understand if there is a correlation between POC flux and fiber flux, Figure 8 shows the flux of fibers normalized to POC. The error was propagated from both POC and fiber flux errors. Ultimately what this normalization shows us is that there was little correlation between plastic and organic matter flux during our collection period. Outside of a few outliers with high error values, the amount of plastic being transported per mmol of POC transported is less than one mm^3. The ratio of plastic: POC also shows no trend with depth.

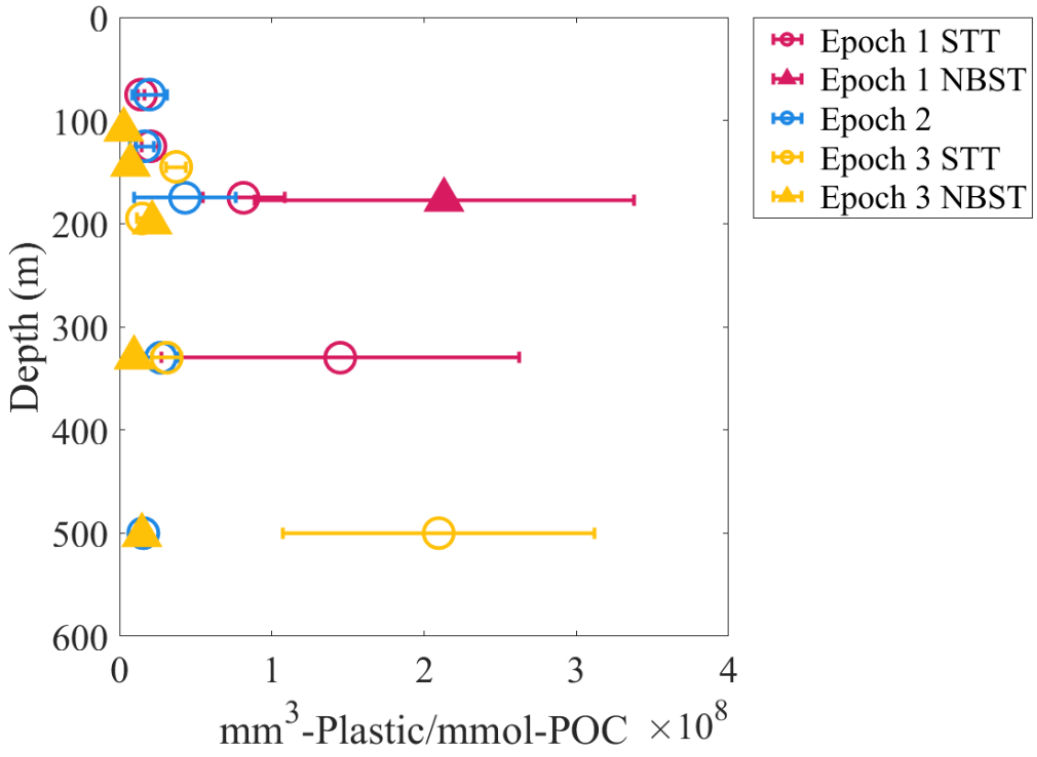

Figure 8: Scatter plot showing the amount of plastic being transported per mmol of POC. Error has been propagated from both POC trap error and fiber flux error.

Our results show no correlation between the flux of plastic and the flux of POC during this event in 2021. The flux of fibers is shown to be unrelated to depth in all three epochs and across both trap types. The correlation between POC and fiber flux was analyzed both visually, by identifying organic material association, and by comparing depth profiles of volumetric and mass flux fluxes of fibers to the flux of POC. These findings demonstrate that the biological carbon pump hypothesis likely had little to no role in the transportation of our fibers to depth. Disaggregation, hypothesis #3, could have occurred which would impact our visual identification of fibers within aggregates. However, we would expect to still see a correlation between fiber

flux and POC flux. Physical mixing dynamics caused by storms and converging currents within the eddy are most likely to have had a large effect on the transport of our samples to depth, although more studies are needed to determine if physical mixing is the primary driver of plastic transportation outside of mesoscale eddies.

CHAPTER 3

CHEMICAL AND PHYSICAL CHARACTERIZATION OF WEATHERED, MARINE MICROPLASTIC FIBERS

3.1. Introduction

Throughout our field observations detailed in Chapter 2, we utilize a suite of methods to improve our understanding of the mechanisms driving vertical microplastic transport and fate in the ocean. Our laboratory experiments aim to answer the following key questions that arose after our field campaign: 1) could the collection methods have disaggregated plastics from natural particles, 2) could the fibers be sinking without being associated with natural particles, and 3) what were the fibers made of?

This study is one of the first to use sediment traps to capture the plastic flux from the mixed layer to the mesopelagic. Drifting sediment traps are a tool used to measure the flux of sinking particles in the euphotic and upper mesopelagic zones in the ocean (Gardner, 1977; Estapa et al., 2021). Measuring a vertical profile of plastic flux allows for comparison to sinking organic material and can provide insight as to how plastic is transported in the water column. In this study, we focused solely on fibers as they were the only shape of microplastic that was consistently found in our samples. This is consistent with the Lenaker et al. (2019) study which cited fibers as the most commonly occurring type of plastic found in the mid-water column. One of our assumptions in our field observations is that the collection methods did not disaggregate plastics from natural particles. Polyacrylamide gel collectors have been utilized to collect and preserve intact sinking aggregates in numerous studies (Ludsgaard 1995; Waite and Nodder 2001; McDonnell and Buesseler, 2010; Durkin et al., 2015). While none of these studies indicate

disaggregation within the gel collectors, we performed a series of experiments to determine if the density difference between plastic and organic material could have stripped the fibers from the natural aggregates.

The second hypothesis introduced in Chapter 2 is the physical mixing hypothesis. Through this hypothesis, we explore the idea that there was minimal relationship between the BCP and plastic transport out of the surface ocean. As detailed in Chapter 1, modeling studies have shown that wind, stratification, and geostrophic currents all play a role in both the vertical and horizontal movement of microplastics (Chevalier et al., 2023). Additionally, mesoscale eddies may cause microplastics to distribute throughout the water column due to geostrophic currents (Vega-Moreno et al., 2021). Sediment traps isolate sinking particles from the more numerically abundant non-sinking particles, indicating that all of our fibers were actively sinking at the time of collection. We isolated a subset of our samples and removed them from their polyacrylamide gel collectors to determine whether or not our fibers could be sinking without being associated with natural particles.

Our third series of laboratory experiments was designed to answer the question: what were the fibers made of? Particles can be identified as plastic in several ways. The most used methods are Raman Spectroscopy (Enders et al., 2015) and Fourier Transform Infrared (FTIR) Spectroscopy (Harrison et al., 2012). Both methods result in spectra of individual microplastics which are used to identify the polymer. Drawbacks to these methods are that they have the potential to identify dyes used on the particle rather than the particle itself, they don't work well on weathered particles, and they're expensive to operate. Color analysis is often used as a proxy for plastic identification (Vega-Moreno et al., 2021), considering that anthropogenic coloring can allow researchers to visually identify if a material is anthropogenic. The drawback of this is that

it often underestimates the number of plastic particles by only identifying those with bright or unnatural coloring or overestimates plastic particles if non-synthetic anthropogenic fibers are present. Additionally, particles may be identified as either synthetic or non-synthetic by utilizing hot needle tests. This test works by superheating a needle or a filament and touching it to the particle to see if it melts (synthetic) or has no response (non-synthetic, such as cotton or wool) (Beckingham et al., 2023).

3.2. Gel Disaggregation Tests

The association between sinking plastic and sinking organic particles has yet to be thoroughly quantified in observational studies (Yoshitake et al., 2023). One of the benefits of utilizing gel collectors at the base of sediment traps is the ability to visualize particles in the orientation they were in when collected, preserving fragile aggregates more successfully than other methods. This allowed us to determine whether the plastic fibers were attached or associated with these aggregates as has been theorized in the literature (Long et al., 2015; Yoshitake et al., 2023).

Field observations detailed in Chapter 2 showed almost no organic matter-fiber association. We conducted laboratory experiments to determine if the density gradient within the polyacrylamide gel collectors drove the disaggregation of fibers and organic matter after samples were collected. The consumer-grade polyester thread was cut into approximately 1 cm pieces and placed in seawater-filled roller tanks (Shanks & Edmondson, 1989) for 24 hours to facilitate natural unraveling in a simulated ocean environment. After unraveling, these threads were placed in an Atlas Suntest CPS+ sunlight simulator for four hours to realistically simulate UV degradation due to being in the euphotic zone, as degraded plastics may interact with aggregates

differently than the original material. This exposure time visibly bleached fibers without burning them. Afterwards, these UV-treated fibers were incorporated into aggregates of three different types of living algal cultures, *Diacronema lutheri*, *Tisochrysis lutea*, *Chaetoceros mulleri* using a roller tank for 24 hours. These phytoplankton were acquired from the University of Maine Darling Marine Center hatchery.

The resulting aggregates were pipetted into separate dishes of 0.2 μm filtered seawater and imaged to ensure the incorporation of fibers. The design of the sediment traps used in the field deployments described in Chapter 2 was mimicked by overlaying filtered seawater on the gels and manually mixing the top centimeter of gel to capture the dynamics of the seawater-gel interface, this was left to settle for 1-2 hours before adding aggregates. The aggregates were pipetted into and allowed to sink through the filtered seawater and then settle into the gels before being re-imaged to look for plastic disaggregation at scales which would have explained the absence of fibers in aggregates seen in the samples. The gels were left to sit at room temperature for 48 hours before reimaging.

During each imaging, a digital caliper (INSIZE Mini) was used to measure the sinking depth of the aggregates. This was expected to increase over time as the overlayed filtered seawater was mixed with the gel and lowered the gel density. Images were taken at time points of 0, 24, and 48 hours. After the 48-hour mark, gels were frozen at -15C for several days. Lab-generated gels were frozen and thawed to mimic the storage and handling conditions of the samples. They were thawed for an additional 48 hours before reimaging. Despite some reorientation and movement after the thawing process, all imaged samples (n= 10 or 12 depending on phytoplankton type) of aggregates and plastics stayed intact in all three phytoplankton aggregate types. Following the criteria of organic matter association used in

identifying fibers with organic matter, there was no difference in organic matter association in the laboratory tests. It is important to note that the aggregates were extremely fragile in filtered seawater and easily disaggregated during the transfer process. Many of these fibers that were disaggregated during handling did not have evidence of organic matter attachment.

A. 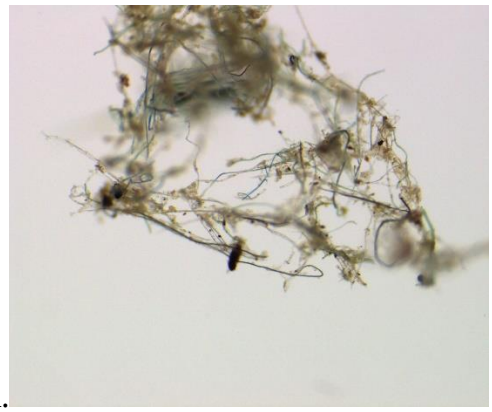 B. 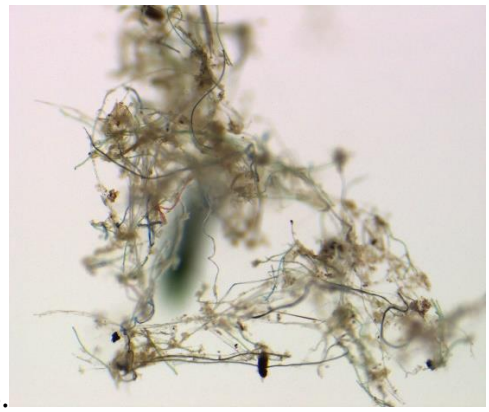

Figure 9: Freeze/thaw test results on an aggregate of *Diacronema lutheri.* Image a shows fiber aggregates in gels before freezing (t = 24) and image b shows fiber aggregates after thawing for 48 hours.

While the type of phytoplankton used did not influence disaggregation within the gels, the aggregates formed were visually very different and required different levels of care when transporting between the tanks and the gels. *Tisochysis lutea* created densely packed balls of fibers with minimal organic matter whereas both *Chaetocerous mulleri* and *Diacronema lutheri* created larger, looser aggregates similar to the one shown in Figure 9. *Chaetoceros mulleri* is a type of diatom, and *Diacronema lutheri* and *Tisochysis lutea* are dinoflagellates, one of the major groups of phytoplankton that produce transparent exopolymers (TEP). The production of TEP promotes particle stickiness and has been investigated as a factor in plastic aggregation and vertical transport (Passow, 2002; Galgani et al., 2022). These observations show that the phytoplankton communities during our deployments could have had a role in disaggregation in

the water column and are often overlooked when considering the modeling of vertical transport of plastic.

3.3. Settling Velocity Tests

Fibers found in gel traps were not associated with organic matter, implying that they were negatively buoyant. We confirmed this using a subset of fibers from gels for settling velocity measurements. The purpose of these measurements was to determine if collected fibers were negatively buoyant and if their sinking velocity was similar to natural aggregates. Between 15% and 20% (n = 20-30) of the total fibers in each gel were removed using a volumetric pipette and placed in a container with MilliQ and stirred to dissolve the gel. Fibers were manually removed from the dissolved gels using forceps and transferred into a high-walled 300mL glass dish containing MilliQ. This process was repeated 3-4 times until the salinity of the rinsing water was equal to 0. Because the gel contained 70 ppt NaCl, ensuring that the rinse water was salt-free was treated as a proxy for the removal of gel from the samples. Finally, fibers were rinsed with the same 39.65 ppt artificial seawater used in settling column runs (described below).

Fibers were then allowed to settle out of a wide-bore glass pipet into the upper 2 cm of a 1”x1”x18” settling column. The placement of fibers into the settling column, rather than their injection, ensured that there was no initial velocity imparted to the fibers during introduction. Convection in the column was monitored using food coloring dissolved in 39.65 ppt artificial seawater that was injected into the column at the surface and allowed to disperse to visualize any lateral water movement. This procedure was repeated as necessary until the column showed no evidence of convective currents. Additionally, the temperature difference between the air and column was measured and required to be less than 1°C before each run to ensure minimal

convection. A salinity of 39.65 ppt was chosen to match the in-situ density at 330 m. Videos of sinking fibers were captured using a ZEISS Stemi 2000-C model microscope on 12.5x magnification with a ZEISS Axiocam 208 color camera attachment using an arm to turn the system on its side. Videos were collected halfway down the settling column to capture fibers at their terminal velocity and measure their orientations. The distance traveled was measured using ImageJ software and measurements were determined using a pixel: mm ratio calculated using a 5 mm graticule. The experimental data are shown in Table A.1.

Fibers' average sinking speeds ranged from 20 to 80 meters per day. Sinking velocities did not significantly vary as a function of the depth of collection, trap type, or epoch. All fibers tested were negatively buoyant in water matching the mean in-situ density at the collection site at 330 m depth. Samples with evidence of convection, abnormally fast sinking near the edges, or sinking near edges and rising in the center of the column, were excluded from the results. Recordings showed that fibers had maintained a steady velocity throughout the measurement screen.

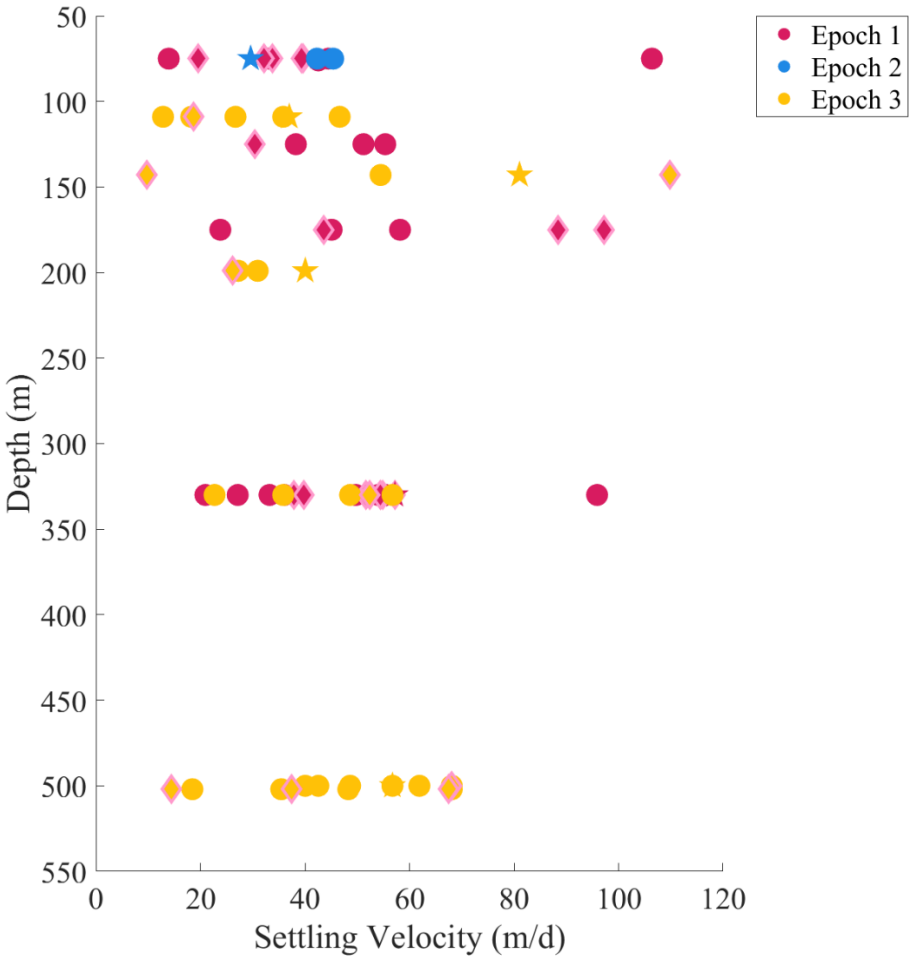

Figure 10: The figure shows the settling velocity of fibers from each epoch and trap depth. Orientations are noted as being vertical (dot), horizontal (diamond), or tangled (star). Several samples from epoch 2 were removed due to convection in the column.

The fibers, when isolated by convective currents, sank at similar speeds as organic matter in the water column at the same approximate depth (Romanelli et al., *in prep*). It is worth noting that the compression or thermal contraction of fibers with increasing depth could theoretically change their density, and ultimately their sinking speeds in the natural environment, although

there is little literature on the compressibility of microfibers in the ocean. As shown in Figure 10, fiber orientation was not related to the terminal velocity of the fibers.

3.4. Composition Analysis

3.4.1 FTIR Analysis

The primary goal of this analysis was to determine the chemical composition of the fibers. The bulk fibers, handpicked from the two brine tubes, were used for this analysis as they were not affected by residual gel that could have potentially influenced the analysis. Our bulk fiber samples were manually removed from filters and placed into clean, 24-well, glass-bottom well plates and underwent a treatment of 33% hydrogen peroxide to ensure organic matter removal.

The composition of the fibers was determined by μ-FTIR using a Thermo Nicolet 380 Fourier Transform Infrared Spectrometer using an ATR cell with a germanium (Ge) crystal from SensIR at Large Lakes Observatory by UM-Duluth. Fiber spectra were evaluated using an OPUS polymer library of plastics, which notably does not include spectra of weathered fibers. Our fibers were challenging to handle manually due to their small size and allowed μFTIR analysis of only 20 of them. The FTIR analysis on the bulk fibers was largely inconclusive due to the small size of the particles and the high degree of weathering. Of the 20 that were measured, 19 fibers were identified as plastic, and the polymers are shown in Figure 11.

The marine environment has been shown to weather plastic particles much more than freshwater or dry ecosystems (Fernández-González et al., 2020). Studies conducted on plastic pellets in numerous environments show notable changes to the IR spectra of most polymers of plastic in just 28 days (Fernández-González et al., 2020). As our samples were collected between

75 and 502 meters in the ocean, they likely underwent even more weathering. The hydrogen peroxide treatment also would have oxidatively weathered the plastics and likely contributed significantly to the poor hit quality of our samples.

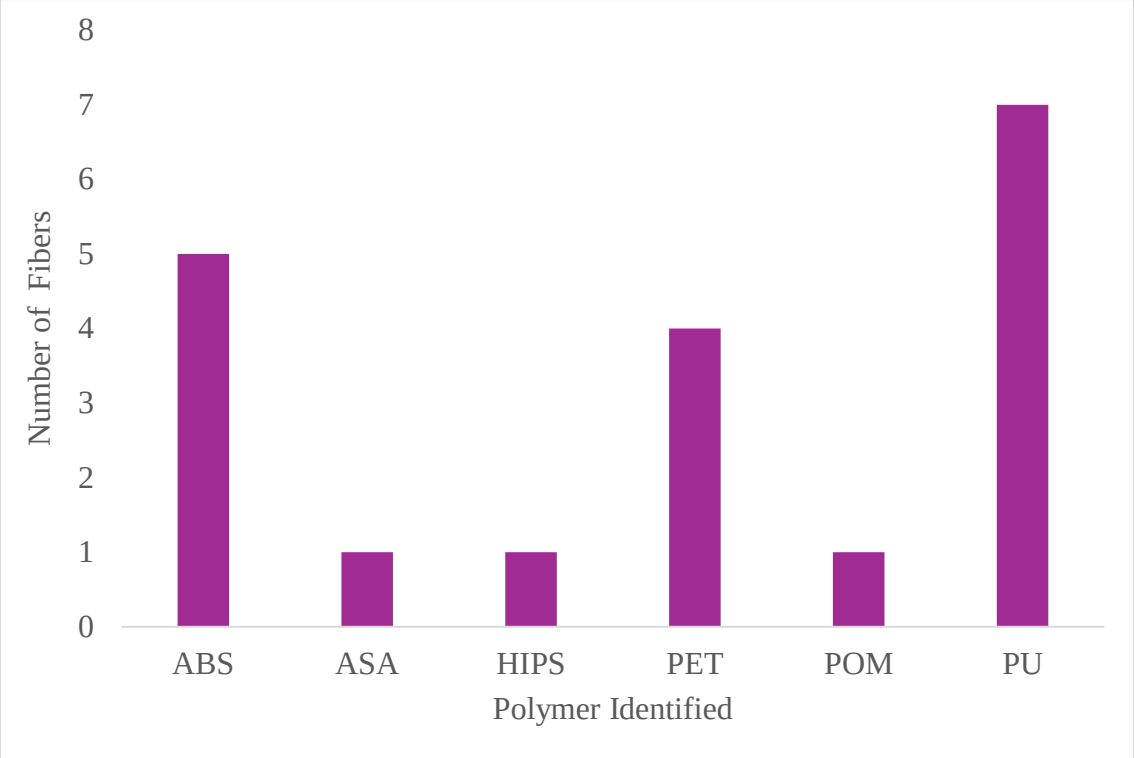

Figure 11: Polymer types identified in samples using FTIR were acrylonitrile butadiene styrene (ABS), acrylonitrile styrene acrylate (ASA), high-impact polystyrene (HIPS), polyethylene terephthalate (PET), polyoxymethylene (POM), and polyurethane (PU).

The polymers included polyethylene terephthalate (PET), acrylonitrile butadiene styrene (ABS), polyurethane (PU), and polyoxymethylene (POM). All identified polymers are negatively buoyant in seawater (SOURCE). The most environmentally stable of the common plastics is PET due to its ring structure (Fernández-González et al., 2020) and it ultimately gave the most confident readings. ABS is a type of thermoplastic, usually rigid, and used in materials such as consumer electronics and 3-D printing. Additionally, the weathering of styrene monomers has

been shown to form carbonyl groups in the 1500-1800 cm^{-1} and hydroxyl groups at 3000-3800 cm^{-1} in the FTIR spectra, leading to the broadening of these regions (Shi et al., 2019). Our spectra showed considerable differences in both regions when compared to the unweathered spectra of the same particles. The identification confidence of our spectra was considerably lower for the three styrene polymers (ABS, HIPS, and ASA). While they were all registered as a type of styrene, the likely weathering of the spectra lowers our confidence in the exact polymer type. All spectra and their classifications can be found at 10.5281/zenodo.10938649.

3.4.2. Hot Needle Testing

Hot needle testing was done in the laboratory on a subset of 12 fibers from the bulk traps that were large enough to handle using a probe superheated by a butane torch (Lenk Model 65 Lab Burner) in increments of 20 seconds. We adopted the criteria recommended by Beckingham et al. (2023) in identifying whether a fiber is plastic:

1) A positive result shows a melt, softening, or significant bend/curl behavior; and

2) No response or a movement/waver behavior with no shape change is a negative result.

Of the 12 fibers tested, 10 of these were categorized as plastic, and 2 had no visible response. All fibers that were removed from the polyacrylamide gel collectors and rinsed from residual gel for this test (n=24) showed no response. As we are the first to utilize polyacrylamide gel collectors for microplastic collection, we are unsure as to any effects they have on hot needle testing methods.

3.4.3 Color Analysis

The color for each of the fibers found in the gel collectors was identified manually using a ZEISS Stemi 2000-C model microscope. Of the 1,400+ fibers collected, 50% were a shade of

blue and 30% were black. This is consistent with other surveys of microplastics which include color (Herrera et al., 2019; Vega-Moreno et al., 2021). The four fibers classified as "undetermined" (Figure 12) were a nearly transparent grey color which could have potentially been organic. The proportion of colors stayed similar when looking at individual traps, indicating that it is unlikely fibers found in each trap were from the same source material.

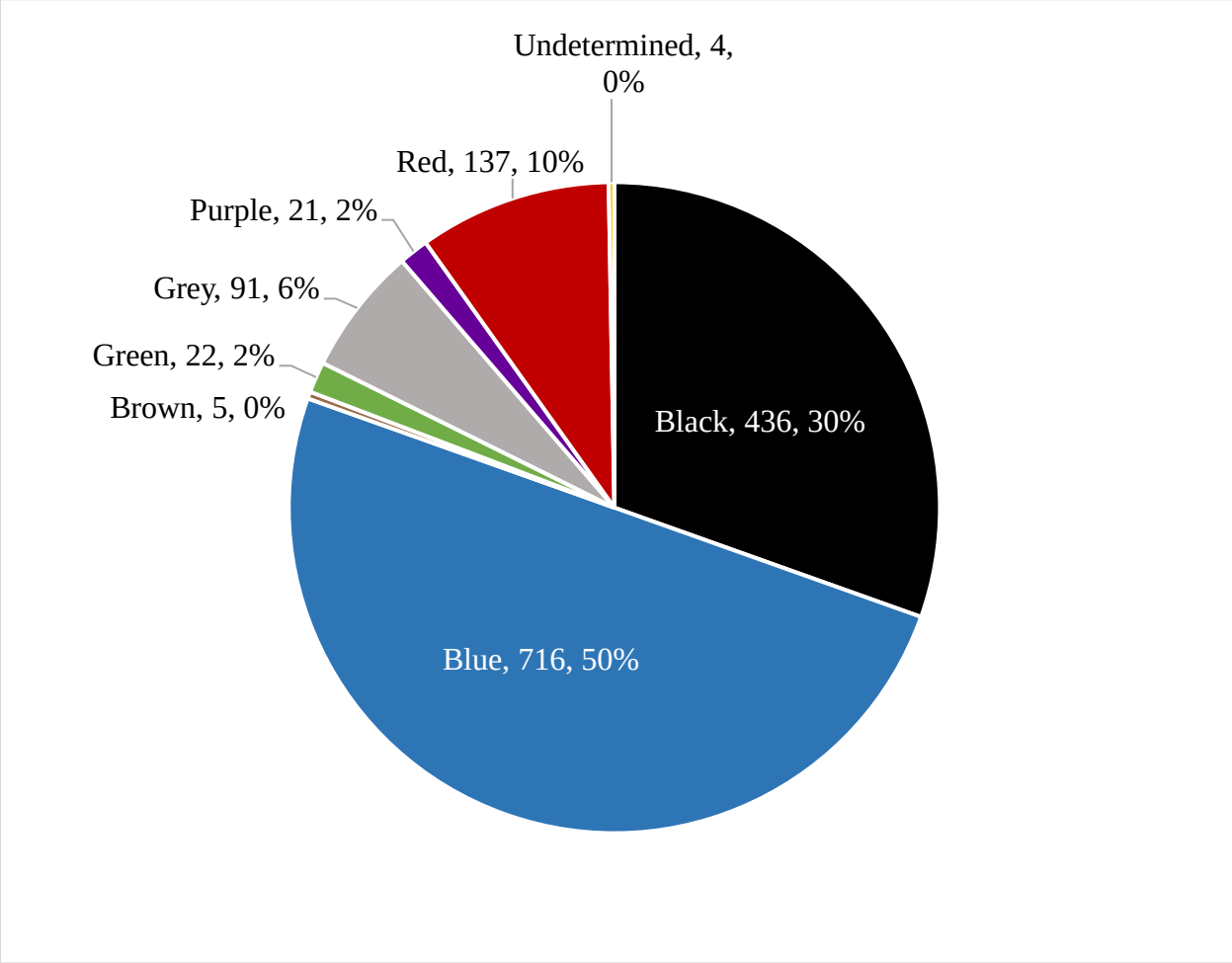

Figure 12: Color analysis of all collected fibers. Most fibers were a shade of blue or black, although seven different colors of fibers were recorded.

3.5. Conclusions

The key questions that arose after our field campaign were: 1) could the collection methods have disaggregated plastics from natural particles, 2) Could the fibers be sinking without being associated with natural particles, and 3) what were the fibers made of?

Our tests of the polyacrylamide gel collectors were shown to preserve fibers in aggregates dominated by both diatoms and dinoflagellates, making them useful tools in the collection of sinking microplastics. These collectors can aid in determining the mechanism of transport of fibers to the mesopelagic by allowing for the visual identification of fibers and organic matter.

Measuring the settling velocity of our fibers showed they were negatively buoyant and had sinking velocities on the same order of magnitude as organic aggregates. However, the movement of these fibers was sensitive to internal currents within the settling column. This test highlights the need to understand the physical behavior of these particles during both vertical and horizontal transport in the water column to accurately model their distribution.

Three methods were used to identify these fibers as plastic. The FTIR results of these small, weathered fibers showed low confidence in identifying the polymer composition of the samples. The spectra show broadened peaks in the carbonyl and hydroxyl groups, consistent with a high degree of weathering. Of the subset conclusively sampled, 80% (n= 20) were determined to be plastic. The hot needle test on the bulk fibers showed 58% (n= 12) met our criteria for plastic. The color analysis of all fibers in the gel collectors (n = 1404) was consistent with several other plastic surveys.

Ultimately, our laboratory tests show that our collection methods did not cause disaggregation between plastic and natural particles and that fibers can be transported independently of natural aggregates. The weathering of plastics creates challenges with polymer identification as it affects FTIR spectra, and few spectra libraries include weathered plastics which leads to low confidence in identification. As fibers are one of the most dominant plastic types found in the mesopelagic, modern plastic identification methods need to be improved upon to determine the composition of small, highly weathered fibers more accurately.

CHAPTER 4

BROADER IMPACTS OF VERTICAL MICROPLASTIC TRANSPORT IN THE OPEN OCEAN

Microplastics are found across nearly every ecosystem on Earth. While buoyant plastic is prevalent in deep-sea sediments and at all depths in the ocean, the mechanisms of the vertical transport of microplastics in the ocean remain poorly understood. Models often utilize the density of particles to track their vertical distribution (Vega-Moreno et al., 2021; Chevalier et al., 2023). However, several studies have indicated that the density of particles, including microplastics, impacts vertical distribution less than shape and size (Stemmann & Boss, 2012; Galgani et al., 2022). This indicates that models of plastic transport in the ocean should prioritize these parameters over polymer density.

Additionally, the biological carbon pump (BCP) is thought to have a role in transporting microplastics and particulate organic carbon (POC) out of the surface ocean. This transport could be via biofilm formation, marine snow aggregates, or ingestion and egestion by zooplankton. Laboratory studies of all three mechanisms show that they are all likely to rapidly increase the settling velocities of microplastics (Gaylarde et al., 2023; Yoshitake et al., 2023; Cole et al., 2016). However, the vertical distribution of plastics in the open ocean is significantly understudied and observational data overall is lacking. Observational studies have shown substantial biofilms on microplastics, but none of the mechanisms demonstrated in the lab have been quantified or observed in the environment.

Microplastics have the potential to influence the BCP by affecting the reproductive potential and growth rates of zooplankton, which are key players in carbon transport (Cole et al., 2016; Steinberg & Landry, 2017). Microplastics may also alter the physical properties of sinking

aggregates, leading to increased rates of disaggregation and resuspension of both carbon and plastic into the water column (Cole et al., 2016). This process keeps both carbon and plastic accessible to marine life, potentially exacerbating the impacts of plastic pollution on mesopelagic ecosystems by increasing the concentrations of microplastics at depth. Thorough research into the role of environmentally relevant plastic concentrations in marine snow disaggregation is needed to further understand the impacts of this plastic-driven disaggregation. Understanding the mechanisms of vertical plastic transport is important for understanding the ecosystems being impacted by things such as psuedostarvation, the leaching of endocrine disrupting chemicals, and the transportation of "forever chemicals" throughout the water column and the food chain.

Our observational study had two objectives. The first objective was to quantify the vertical flux and distribution of sinking microplastics within an isolated water mass associated with a mesoscale eddy. The second objective was to determine if BCP processes such as the transport of POC after a phytoplankton bloom were responsible for enhancing the flux of microplastics, as predicted by models. To determine this association, we compared the rate of transport (flux) of POC to the microplastic flux, examined whether sinking plastics were associated with sinking natural particles, measured fiber sinking speeds, and assessed properties such as plastic particle size to assess whether plastics were being fragmented in a systematic way by non-BCP processes.

We measured fluxes of plastic ranging from 0.5 $\mu m^3\ m^{-2}\ d^{-1}$ and 7 $\mu m^3\ m^{-2}\ d^{-1}$ across all depths and epochs sampled. There were no clear depth trends in microplastic flux. Fibers between 0-3 μm^3 were most prevalent at all depths. This finding shows that there was no size-specific mechanism transporting fibers or fragmenting them at the depths that we sampled, 75 – 500 m. This is consistent with other studies of the vertical distribution of fibers in the water

column (Lenaker et al., 2019; Galgani et al., 2022). Numerous studies before this one infer that there must be a size-specific mechanism for transporting microplastics out of the surface ocean (Cózar et al., 2014; Erikson et al., 2014). This process likely takes place closer to the surface as its effects are not seen below the mixed layer.

To address objective #2 above, we proposed to test 3 hypotheses for how plastic fibers are transported vertically in the water column. In the first of these, the "biological carbon pump hypothesis", we take the concepts of previous laboratory studies of plastics in the biological carbon pump and apply them directly to our sample site. In this scenario, microplastics would be stuck to marine snow, covered in biofilms, or incorporated into zooplankton fecal pellets. If this hypothesis is correct, each of these plastic-containing particle types would be visually identifiable and retained in the polyacrylamide gel collector. However, of the 1404 fibers imaged within our gel collectors, only 6% of them had visually attached organic matter and less than 10 fibers were incorporated into an aggregate, despite the prevalence of aggregates in the samples. Instead, we observed that most fibers were separate from organic matter and visually clean. Therefore, this evidence supports abandoning this hypothesis as an explanation for the observations made here.

Through the second hypothesis proposed, the "physical mixing hypothesis", we consider the physical dynamics of the collection site as being the primary driver of the transport of microplastic fibers. Within the core of a retentive, anti-cyclonic eddy, there was potentially a higher accumulation of microplastics due to converging currents. These converging currents additionally could have driven the downward transportation of fibers as anticyclonic eddies have been shown to promote downwelling (Mizobata et al., 2002). Furthermore, the weathering of plastic fibers can change their buoyancy, causing them to become negatively buoyant and able to

sink even without being aggregated into larger particles. As our study found no significant correlation between the flux of microplastics and the flux of POC during the spring bloom event, this hypothesis is likely to have been a primary driver of plastic transport during our collection period.

To test the likelihood of hypothesis two, we measured the settling velocity of a subset of our fiber samples. This test showed that the fibers we collected were negatively buoyant and had sinking velocities on the same order of magnitude as organic aggregates. Biofouling can affect the hydrophobicity and buoyancy of microplastics by modifying the volume: density ratio (Gaylarde et al., 2023). Additionally, weathering can change the buoyancy of fibers, regardless of the properties of the pure polymer. Our settling velocity speeds were measured while isolated from other currents or mixing through the water column. However, these experiments provide support that physical processes alone could be enough to transport plastics, even in the ocean interior.

Despite the lack of correlation between the flux of microplastics and POC shown in our dataset, marine snow could still have played a role in the vertical transport of fibers before being disaggregated by physical processes such as turbulence-driven shear, or biological processes such as zooplankton feeding. This is what we have coined as the “disaggregation hypothesis” or hypothesis three. This would have required a supply of aggregate-associated microplastics (hypothesis #1) at some point in the past, before the sample collection period, and there was no evidence of plastic and POC following the same depth trends. While hypothesis 3 is not strongly supported, it cannot be ruled out.

Overall, this study utilized novel methods to provide new insights into the vertical distribution and transport mechanisms of microfibers in the ocean. We highlight the importance

of considering trap type and collection site during observational studies of mesopelagic microplastic pollution. Ultimately, further research into the transport mechanisms of microplastics is needed to accurately model concentrations and identify affected ecosystems. This is one of the first studies utilizing sediment traps to isolate sinking microplastics, and the first study to our knowledge to utilize NBSTs and polyacrylamide gel collectors for microplastic collection. The isolation of sinking plastics allows us to quantify the vertical flux of plastic. Traditional methods of plastic collection such as Manta trawls or bulk filtering, quantify the overall abundance of plastic at specific depths, regardless of the plastic's motion in the water column. This study also highlighted the impact of sediment trap types on the size of fibers collected in samples. NBSTs collected larger particles than STTs at the same depths. This could be due to trap type influencing the size of fibers collected or the overall patchiness of plastic flux. As sediment traps become integrated into microplastic collection methods, potential discrepancies between NBSTs and STTs need to be further studied.

Rigorous laboratory tests showed that gels preserved fibers in aggregates dominated by both diatoms and dinoflagellates. There was no measurable disaggregation of particles after being stored at room temperature for 48 hours or after being frozen and thawed, although the freezing and thawing showed slight rearrangements. There was no difference observed between the three types of phytoplankton used for aggregation, allowing for the collection and preservation of extremely fragile aggregates.

In addition to the gel collectors, laboratory tests highlighted the challenges of identifying the composition of small, highly weathered fibers. While techniques such as FTIR spectroscopy are highly successful for less weathered microplastics and those captured in 330um Manta trawls, they are expensive and do not always provide conclusive results for highly weathered

particles. Using this test, we were able to successfully identify several different types of plastic polymers, all of which were denser than seawater. Particles captured within the eddy core waters during our sampling (identified as being below 200m) were likely there for at least 20 days before sampling (Johnson et al., 2024). Weathering studies conducted by Fernandez-Gonzalez et al. (2021) showed substantial differences in FTIR spectra after only 28 days of being exposed to the marine environment. We were unable to age our fiber samples, but we suspect a high degree of weathering due to their presence in the offshore environment and the broad carbonyl and hydroxyl groups present in the spectra, indicating that weathering had caused the creation of various degradation products.

To provide a complementary determination of fiber composition, we recorded the fiber colors and conducted hot needle testing to identify fibers as plastic. By recording the color of fibers, we were able to determine if fibers likely came from the same source or if they were consistent with contamination from our equipment. For example, yellow strands found in one of the bulk samples were removed from analysis due to being the same color and morphology as the rope that was used to tether the sediment traps. We were also able to determine that the proportion of colors recorded was consistent with several other plastic surveys which included color as a proxy for synthetic material (Lenaker et al., 2019; Vega-Moreno et al., 2021). This test has several drawbacks, including preferential sampling of brightly colored fibers, lack of knowledge of the composition of the material, and the inability to distinguish between anthropogenic fibers and plastic fibers.

Our hot needle tests showed that over half of the fibers tested melted, while several showed no response or became brittle and broke. Hot needle tests when conducted using

objective criteria (Beckingham et al., 2023) are a cost-effective complement to advanced analyses and have been used in this study and others after FTIR analysis of weathered particles. The incorporation of this test into our analyses improved confidence in our FTIR and color analysis results.

Overall, this study contributes to the understanding of the transport and fate of microplastics throughout the water column. While there was no evidence that the BCP played a role in the transport of microplastics at our sample site, comparisons to different mesoscale features are needed to fully understand the relationship between POC transport and microplastics. If anticyclonic eddies concentrate microplastics and promote their transportation into the mesopelagic (hypothesis #2), mesoscale processes need to be considered in future models of plastic transport. Additionally, the BCP may still play a role in the transport of plastics outside of these features and this study provides a suite of novel approaches and methods to observationally determine and quantify this role.

BIBLIOGRAPHY

Bakir, A., O'Connor, I. A., Rowland, S. J., Hendriks, A. J., & Thompson, R. C. (2016). Relative importance of microplastics as a pathway for the transfer of hydrophobic organic chemicals to marine life. Environmental Pollution, 219, 56–65. https://doi.org/10.1016/j.envpol.2016.09.046

Beckingham, B., Apintiloaiei, A., Moore, C., & Brandes, J. (2023). Hot or not: Systematic review and laboratory evaluation of the hot needle test for microplastic identification. Microplastics and Nanoplastics, 3(1), 8. https://doi.org/10.1186/s43591-023-00056-4

Brach, L., Deixonne, P., Bernard, M.-F., Durand, E., Desjean, M.-C., Perez, E., van Sebille, E., & ter Halle, A. (2018). Anticyclonic eddies increase accumulation of microplastic in the North Atlantic subtropical gyre. Marine Pollution Bulletin, 126, 191–196. https://doi.org/10.1016/j.marpolbul.2017.10.077

Chen, Q., Allgeier, A., Yin, D., & Hollert, H. (2019). Leaching of endocrine disrupting chemicals from marine microplastics and mesoplastics under common life stress conditions. Environment International, 130, 104938. https://doi.org/10.1016/j.envint.2019.104938

Chevalier, C., Vandenberghe, M., Pagano, M., Pellet, I., Pinazo, C., Tesán Onrubia, J. A., Guilloux, L., & Carlotti, F. (2023). Investigation of dynamic change in microplastics vertical distribution patterns: The seasonal effect on vertical distribution. Marine Pollution Bulletin, 189, 114674. https://doi.org/10.1016/j.marpolbul.2023.114674

Clevenger, S. J., Benitez-Nelson, C. R., Roca-Martí, M., Bam, W., Estapa, M., Kenyon, J. A., Pike, S., Resplandy, L., Wyatt, A., & Buesseler, K. O. (2024). Carbon and silica fluxes during a declining North Atlantic spring bloom as part of the EXPORTS program. Marine Chemistry, 258, 104346. https://doi.org/10.1016/j.marchem.2023.104346

Cole, M., Lindeque, P. K., Fileman, E., Clark, J., Lewis, C., Halsband, C., & Galloway, T. S. (2016). Microplastics Alter the Properties and Sinking Rates of Zooplankton Faecal Pellets. Environmental Science & Technology, 50(6), 3239–3246. https://doi.org/10.1021/acs.est.5b05905

Cózar, A., Echevarría, F., González-Gordillo, J. I., Irigoien, X., Úbeda, B., Hernández-León, S., Palma, Á. T., Navarro, S., García-de-Lomas, J., Ruiz, A., Fernández-de-Puelles, M. L., & Duarte, C. M. (2014). Plastic debris in the open ocean. Proceedings of the National Academy of Sciences, 111(28), 10239–10244. https://doi.org/10.1073/pnas.1314705111

Durkin, C. A., Buesseler, K. O., Cetinić, I., Estapa, M. L., Kelly, R. P., & Omand, M. (2021). A Visual Tour of Carbon Export by Sinking Particles. Global Biogeochemical Cycles, 35(10), e2021GB006985. https://doi.org/10.1029/2021GB006985

Egger, M., Sulu-Gambari, F., & Lebreton, L. (2020). First evidence of plastic fallout from the

North Pacific Garbage Patch. Scientific Reports, 10(1), Article 1. https://doi.org/10.1038/s41598-020-64465-8

Enders, K., Lenz, R., Stedmon, C. A., & Nielsen, T. G. (2015). Abundance, size and polymer composition of marine microplastics ≥10μm in the Atlantic Ocean and their modelled vertical distribution. Marine Pollution Bulletin, 100(1), 70–81. https://doi.org/10.1016/j.marpolbul.2015.09.027

Eriksen, M., Lebreton, L. C. M., Carson, H. S., Thiel, M., Moore, C. J., Borerro, J. C., Galgani, F., Ryan, P. G., & Reisser, J. (2014). Plastic Pollution in the World's Oceans: More than 5 Trillion Plastic Pieces Weighing over 250,000 Tons Afloat at Sea. PLOS ONE, 9(12), e111913. https://doi.org/10.1371/journal.pone.0111913

Estapa, M., Valdes, J., Tradd, K., Sugar, J., Omand, M., & Buesseler, K. (2020). The Neutrally Buoyant Sediment Trap: Two Decades of Progress. Journal of Atmospheric and Oceanic Technology, 37(6), 957–973. https://doi.org/10.1175/JTECH-D-19-0118.1

Estapa, M., Buesseler, K., Durkin, C. A., Omand, M., Benitez-Nelson, C. R., Roca-Martí, M., Breves, E., Kelly, R. P., & Pike, S. (2021). Biogenic sinking particle fluxes and sediment trap collection efficiency at Ocean Station Papa. Elementa: Science of the Anthropocene, 9(1), 00122. https://doi.org/10.1525/elementa.2020.00122

Fernández-González, V., Andrade-Garda, J. M., López-Mahía, P., & Muniategui-Lorenzo, S. (2021). Impact of weathering on the chemical identification of microplastics from usual packaging polymers in the marine environment. Analytica Chimica Acta, 1142, 179–188. https://doi.org/10.1016/j.aca.2020.11.002

Galgani, L., Goßmann, I., Scholz-Böttcher, B., Jiang, X., Liu, Z., Scheidemann, L., Schlundt, C., & Engel, A. (2022). Hitchhiking into the Deep: How Microplastic Particles are Exported through the Biological Carbon Pump in the North Atlantic Ocean. Environmental Science & Technology, 56(22), 15638–15649. https://doi.org/10.1021/acs.est.2c04712

Gardner, W. D. 1977. Fluxes, dynamics and chemistry of particulates in the ocean. Ph.D. Thesis, Massachusetts Institute of Technology/ Woods Hole Oceanographic Institution Joint Program in Oceanography. 405 pp

Gaylarde, C. C., de Almeida, M. P., Neves, C. V., Neto, J. A. B., & da Fonseca, E. M. (2023). The Importance of Biofilms on Microplastic Particles in Their Sinking Behavior and the Transfer of Invasive Organisms between Ecosystems. Micro, 3(1), Article 1. https://doi.org/10.3390/micro3010022

Harrison, J. P., Ojeda, J. J., & Romero-González, M. E. (2012). The applicability of reflectance micro-Fourier-transform infrared spectroscopy for the detection of synthetic microplastics in marine sediments. Science of The Total Environment, 416, 455–463. https://doi.org/10.1016/j.scitotenv.2011.11.078

Herrera, A., Ŝtindlová, A., Martínez, I., Rapp, J., Romero-Kutzner, V., Samper, M. D., Montoto, T., Aguiar-González, B., Packard, T., & Gómez, M. (2019). Microplastic ingestion by Atlantic chub mackerel (Scomber colias) in the Canary Islands coast. Marine Pollution Bulletin, 139, 127–135. https://doi.org/10.1016/j.marpolbul.2018.12.022

Johnson, L., Siegel, D. A., Thompson, A. F., Fields, E., Erickson, Z. K., Cetinic, I., Lee, C. M., D'Asaro, E. A., Nelson, N. B., Omand, M. M., Sten, M., Traylor, S., Nicholson, D. P., Graff, J. R., Steinberg, D. K., Sosik, H. M., Buesseler, K. O., Brzezinski, M. A., Ramos, I. S., … Henson, S. A. (2024). Assessment of oceanographic conditions during the North Atlantic EXport processes in the ocean from RemoTe sensing (EXPORTS) field campaign. Progress in Oceanography, 220, 103170. https://doi.org/10.1016/j.pocean.2023.103170

Kaiser, D., Kowalski, N., & Waniek, J. J. (2017). Effects of biofouling on the sinking behavior of microplastics. Environmental Research Letters, 12(12), 124003. https://doi.org/10.1088/1748-9326/aa8e8b

Khatmullina, L., & Isachenko, I. (2017). Settling velocity of microplastic particles of regular shapes. Marine Pollution Bulletin, 114(2), 871–880. https://doi.org/10.1016/j.marpolbul.2016.11.024

Kvale, K. F., Friederike Prowe, A. E., & Oschlies, A. (2020). A Critical Examination of the Role of Marine Snow and Zooplankton Fecal Pellets in Removing Ocean Surface Microplastic. Frontiers in Marine Science, 6. https://www.frontiersin.org/articles/10.3389/fmars.2019.00808

Law, K. L., Morét-Ferguson, S., Maximenko, N. A., Proskurowski, G., Peacock, E. E., Hafner, J., & Reddy, C. M. (2010). Plastic Accumulation in the North Atlantic Subtropical Gyre. Science, 329(5996), 1185–1188. https://doi.org/10.1126/science.1192321

Law, K. L. (2017). Plastics in the Marine Environment. Annual Review of Marine Science, 9(1), 205–229. https://doi.org/10.1146/annurev-marine-010816-060409

Lenaker, P. L., Baldwin, A. K., Corsi, S. R., Mason, S. A., Reneau, P. C., & Scott, J. W. (2019). Vertical Distribution of Microplastics in the Water Column and Surficial Sediment from the Milwaukee River Basin to Lake Michigan. Environmental Science & Technology, 53(21), 12227–12237. https://doi.org/10.1021/acs.est.9b03850

Liu, K., Courtene-Jones, W., Wang, X., Song, Z., Wei, N., & Li, D. (2020). Elucidating the vertical transport of microplastics in the water column: A review of sampling methodologies and distributions. Water Research, 186, 116403. https://doi.org/10.1016/j.watres.2020.116403

Long, M., Moriceau, B., Gallinari, M., Lambert, C., Huvet, A., Raffray, J., & Soudant, P. (2015).

Interactions between microplastics and phytoplankton aggregates: Impact on their respective fates. Marine Chemistry, 175, 39–46. https://doi.org/10.1016/j.marchem.2015.04.003

Lundsgaard, C., & Olesen, M. (1997). The origin of sedimenting detrital matter in a coastal system. Limnology and Oceanography, 42(5), 1001–1005. https://doi.org/10.4319/lo.1997.42.5.1001

McDonnell, A. M. P., & Buesseler, K. O. (2010). Variability in the average sinking velocity of marine particles. Limnology and Oceanography, 55(5), 2085–2096. https://doi.org/10.4319/lo.2010.55.5.2085

Mizobata, K., Saitoh, S. I., Shiomoto, A., Miyamura, T., Shiga, N., Imai, K., Toratani, M., Kajiwara, Y., & Sasaoka, K. (2002). Bering Sea cyclonic and anticyclonic eddies observed during summer 2000 and 2001. Progress in Oceanography, 55(1), 65–75. https://doi.org/10.1016/S0079-6611(02)00070-8

Pabortsava, K., & Lampitt, R. S. (2020). High concentrations of plastic hidden beneath the surface of the Atlantic Ocean. Nature Communications, 11(1), Article 1. https://doi.org/10.1038/s41467-020-17932-9

Passow, U. (2002). Transparent exopolymer particles (TEP) in aquatic environments. Progress in Oceanography, 55(3–4), 287–333. https://doi.org/10.1016/S0079-6611(02)00138-6

Provencher, J. F., Vermaire, J. C., Avery-Gomm, S., Braune, B. M., & Mallory, M. L. (2018). Garbage in guano? Microplastic debris found in faecal precursors of seabirds known to ingest plastics. Science of The Total Environment, 644, 1477–1484. https://doi.org/10.1016/j.scitotenv.2018.07.101

Rochman, C., & Tahir, A. (2015). Anthropogenic debris in seafood: Plastic debris and fibers from textiles in fish and bivalves sold for human consumption. Scientific Reports, 5(14340).

Shanks, A. L., & Edmondson, E. W. (1989). Laboratory-made artificial marine snow: A biological model of the real thing. Marine Biology, 101(4), 463–470. https://doi.org/10.1007/BF00541648

Shi, Y., Qin, J., Tao, Y., Jie, G., & Wang, J. (2019). Natural weathering severity of typical coastal environment on polystyrene: Experiment and modeling. Polymer Testing, 76, 138–145. https://doi.org/10.1016/j.polymertesting.2019.03.018

Steinberg, D. K., & Landry, M. R. (2017). Zooplankton and the Ocean Carbon Cycle. Annual Review of Marine Science, 9(Volume 9, 2017), 413–444. https://doi.org/10.1146/annurev-marine-010814-015924

Uurasjärvi, E., Pääkkönen, M., Setälä, O., Koistinen, A., & Lehtiniemi, M. (2021). Microplastics

accumulate to thin layers in the stratified Baltic Sea. Environmental Pollution, 268, 115700. https://doi.org/10.1016/j.envpol.2020.115700

Vega-Moreno, D., Abaroa-Pérez, B., Rein-Loring, P. D., Presas-Navarro, C., Fraile-Nuez, E., & Machín, F. (2021). Distribution and transport of microplastics in the upper 1150 m of the water column at the Eastern North Atlantic Subtropical Gyre, Canary Islands, Spain. Science of The Total Environment, 788, 147802. https://doi.org/10.1016/j.scitotenv.2021.147802

Waite, A. M., & Nodder, S. D. (2001). The effect of in situ iron addition on the sinking rates and export flux of Southern Ocean diatoms. Deep Sea Research Part II: Topical Studies in Oceanography, 48(11), 2635–2654. https://doi.org/10.1016/S0967-0645(01)00012-1

Yoshitake, M., Isobe, A., Song, Y. K., & Shim, W. J. (2023). A Numerical Model Approach Toward a Settling Process and Feedback Loop of Ocean Microplastics Absorbed Into Phytoplankton Aggregates. Journal of Geophysical Research: Oceans, 128(5), e2022JC018961. https://doi.org/10.1029/2022JC018961

APPENDIX

Table A.1. Experimental data from sinking velocity measurements. JCXX indicates which gel the fibers were taken from and the -X indicates the fiber number. All fibers were recorded for the same distance at their terminal velocity. Orientations of the fibers are classified as horizontal (H) = 1, vertical (V) = 2, or tangled/glob = 3.

Name	Start	End	Time (s)	Distance (m)	Velocity (m/s)	Velocity (m/day)	Trap Depth (m)	Orientation (H = 1, V = 2, Glob = 3)
JC5-1	138.4	144.8	6.4	0.00788	0.001231	106.38	75	1
JC5-2	275.8	293.0	17.2	0.00788	0.000458	39.58	75	2
JC5-3	357.2	372.5	15.3	0.00788	0.000515	44.50	75	1
JC5-4	184.5	204.7	20.2	0.00788	0.000390	33.70	75	2
JC5-5	207.6	224.9	17.3	0.00788	0.000455	39.35	75	2
JC5-6	237.1	257.7	20.6	0.00788	0.000383	33.05	75	1
JC5-7	259.1	280.3	21.2	0.00788	0.000372	32.11	75	2
JC5-8	309.7	344.6	34.9	0.00788	0.000226	19.51	75	2
JC5-9	455.0	503.9	48.9	0.00788	0.000161	13.92	75	1
JC6-0	105.0	121.0	16.0	0.00788	0.000493	42.55	76	1
JC6-1	150.0	162.3	12.3	0.00788	0.000641	55.35	125	1
JC6-2	248.3	261.6	13.3	0.00788	0.000592	51.19	125	1
JC6-3	442.8	465.2	22.4	0.00788	0.000352	30.39	125	2
JC6-4	448.2	466.0	17.8	0.00788	0.000443	38.25	125	1
JC7-1	149.0	156.7	7.7	0.00788	0.001023	88.42	175	2
JC7-2	204.8	211.8	7.0	0.00788	0.001126	97.26	175	2

Table A.1. Continued

JC7-3	370.4	386.0	15.6	0.00788	0.000505	43.64	175	2
JC7-4	408.9	424.0	15.1	0.00788	0.000522	45.09	175	1
JC7-5	243.1	254.8	11.7	0.00788	0.000674	58.19	175	1
JC7-6	280.0	308.6	28.6	0.00788	0.000276	23.81	175	1
JC8-1	59.0	66.1	7.1	0.00788	0.001110	95.89	330	1
JC8-3	167.4	179.7	12.3	0.00788	0.000641	55.35	330	1
JC8-4	171.7	183.6	11.9	0.00788	0.000662	57.21	330	3
JC8-5	211.0	222.9	11.9	0.00788	0.000662	57.21	330	2
JC8-6	218.9	231.5	12.6	0.00788	0.000625	54.03	330	1
JC8-7	222.9	235.3	12.4	0.00788	0.000635	54.91	330	2
JC8-8	248.6	261.1	12.5	0.00788	0.000630	54.47	330	2
JC8-9	323.8	337.5	13.7	0.00788	0.000575	49.70	330	1
JC8-10	333.5	352.4	18.9	0.00788	0.000417	36.02	330	1
JC8-11	346.8	364.8	18.0	0.00788	0.000438	37.82	330	2
JC8-12	335.0	367.5	32.5	0.00788	0.000242	20.95	330	1
JC8-13	362.6	375.8	13.2	0.00788	0.000597	51.58	330	2
JC8-14	362.6	387.7	25.1	0.00788	0.000314	27.12	330	1
JC8-15	364.2	381.3	17.1	0.00788	0.000461	39.81	330	2
JC8-16	421.2	441.7	20.5	0.00788	0.000384	33.21	330	1
JC21-1	132.1	148.2	16.1	0.00788	0.000489	42.29	75	1
JC21-2	147.0	162.0	15.0	0.00788	0.000525	45.39	75	1
JC21-3	456.0	479.0	23.0	0.00788	0.000343	29.60	75	3

Table A.1. Continued

JC49-1	180.6	195.2	14.6	0.00788	0.000540	46.63	109	1
JC49-2	194.3	230.8	36.5	0.00788	0.000216	18.65	109	2
JC49-3	254.2	272.6	18.4	0.00788	0.000428	37.00	109	3
JC49-4	336.1	355.1	19.0	0.00788	0.000415	35.83	109	1
JC49-5	337.8	363.3	25.5	0.00788	0.000309	26.70	109	1
JC49-6	391.1	428.4	37.3	0.00788	0.000211	18.25	109	1
JC49-7	452.0	505.0	53.0	0.00788	0.000149	12.85	109	1
JC51-1	100.5	113.0	12.5	0.00788	0.000630	54.47	143	1
JC51-2	117.9	126.3	8.4	0.00788	0.000938	81.05	143	3
JC51-3	181.4	187.6	6.2	0.00788	0.001271	109.81	143	2
JC51-4	142.0	211.8	69.8	0.00788	0.000113	9.75	143	2
JC55-1	171.0	183.0	12.0	0.00788	0.000657	56.74	330	1
JC55-2	256.0	269.0	13.0	0.00788	0.000606	52.37	330	2
JC56-1	40.0	50.0	10.0	0.00788	0.000788	68.08	500	2
JC56-2	97.0	107.0	10.0	0.00788	0.000788	68.08	500	1
JC56-3	180.0	192.0	12.0	0.00788	0.000657	56.74	500	3
JC56-4	186.0	197.0	11.0	0.00788	0.000716	61.89	500	1
JC56-5	204.0	218.0	14.0	0.00788	0.000563	48.63	500	1
JC56-6	232.0	248.0	16.0	0.00788	0.000493	42.55	500	1
JC56-7	344.0	356.0	12.0	0.00788	0.000657	56.74	500	1
JC56-8	358.0	375.0	17.0	0.00788	0.000464	40.05	500	1
JC63-1	297.0	319.0	22.0	0.00788	0.000358	30.95	199	1

BIOGRAPHY OF THE AUTHOR

Mikayla Elizabeth Clark was born in Voorhees, NJ where she lived for 10 years before moving to Ninilchik, Alaska. In 2020, she obtained her Bachelor of Science in Biology with a minor in Environmental Science from the University of Alaska Southeast in Juneau, Alaska. During the COVID-19 pandemic, she worked with the International Arctic Research Center on the *A/V Akademik Tryoshnikov* in the Russian arctic. In 2022, she joined the University of Maine School of Marine Sciences. Mikayla is a candidate for the Master of Science degree in Oceanography in May 2024.